2012-06-18

Detecting Vegetation Recovery Patterns After Hurricanes in South Florida Using NDVI Time Series

Yu Wang
University of Miami, wangyu8722@gmail.com

UNIVERSITY OF MIAMI

DETECTING VEGETATION RECOVERY PATTERNS AFTER HURRICANES IN SOUTH FLORIDA USING NDVI TIME SERIES

By

Yu Wang

A THESIS

Submitted to the Faculty
of the University of Miami
in partial fulfillment of the requirements for
the degree of Master of Arts

Coral Gables, Florida

June 2012

UNIVERSITY OF MIAMI

A thesis submitted in partial fulfillment of
the requirements for the degree of
Master of Arts

DETECTING VEGETATION RECOVERY PATTERNS AFTER HURRICANES IN SOUTH FLORIDA USING NDVI TIME SERIES

Yu Wang

Approved:

_____	_____
Douglas Fuller, Ph.D. Professor of Geography and Regional Studies	Dean of the Graduate School
_____	_____
Shouraseni Sen Roy, Ph.D. Associate Professor of Geography and Regional Studies	Shimon Wdowinski, Ph.D. Research Associate Professor of Marine Geology and Geophysics

WANG, YU (M.A., Geography)

Detecting Vegetation Recovery Patterns After Hurricanes In South Florida Using NDVI Time Series (June 2012)

Abstract of a thesis at the University of Miami.

Thesis supervised by Professor Douglas Fuller.
No. of pages in text. (51)

The Normalized Difference Vegetation Index (NDVI) is one of the most widely used vegetation indexes to measure and monitor plant growth, vegetation cover, and biomass production. A variety of different multispectral satellite systems could provide NDVI time series to examine the long-term vegetation process patterns. The effects of hurricanes on forested ecosystems can range from very minor defoliation of only a few trees to catastrophic blow-down of whole forest. During 2005, two hurricanes hit South Florida, Hurricane Katrina on Aug 25th and Hurricane Wilma on Oct. 24th. Several studies have evaluated the impact of hurricanes on mangroves, but relatively few have analyzed the rates and patterns of recovery from disturbances of mangrove forest and other vegetation using a NDVI time series. This thesis uses NDVI time series from imagery 2001 to 2010 with an 8-day interval derived from the MODIS Terra to detect the recovery rate of mangrove after the two major hurricanes in South Florida. The slope obtained from Ordinary Least Square (OLS) is used to analyze the recovery rates in this thesis. The slope values from OLS were compared between pre-hurricane and post-hurricane periods to show that the most rapid recovery rates were happening in the first years after the 2005 hurricanes events. This research showed that it took around 2 to 3 years for vegetation to recover to normal level in terms of phenological rhythms.

Acknowledgements

This thesis would not have been possible without the guidance and the help of several individuals who in one way or another contributed and extended their valuable assistance in the preparation and completion of this study.

First, I would like to thank Dr. Douglas Fuller, for his patience and guidance throughout the process of creating this thesis. Also, I would like to thank Dr. Shouraseni Sen Roy, for her encouragement and advice at each step. Finally, I would also like to give thanks to Dr. Shimon Wdowinski for serving on my committee.

Special thanks to Eric Behrle for reading this thesis and providing editorial comments.

Lat but not the least, I want to thank my parents, Yan Chen and Yunfeng Wang, as well as my boyfriend, Lin Xing, for all their unconditional support and encouragement.

TABLE OF CONTENTS

Page

List of Figures

List of Tables

Chapter 1

Introduction

Land cover studies using satellite observations have gained much interest especially in recent decades. Remote sensing techniques have provided a range of useful methods that quantitatively measure land change process as on a larger scale with less expense compared with traditional methods, such as field surveys. Several different parameters derived from satellite data have been used in land cover studies such as detecting land cover changes, measuring the loss of water and so forth. The Normalized Difference Vegetation Index (NDVI) calculated from the red and near-infra-red bands, is one of the most widely used vegetation indexes in a variety of vegetation studies such as measuring plant growth or extracting phenological metrics.

The NDVI time series consists of a set of NDVI imagery arranged in chronological order. The raw time series may contain noise manifested as different levels of fluctuations caused by the cloudiness, data transmission errors, incomplete or inconsistent atmospheric correction, or bi-directional effects. To obtain a higher quality NDVI time series, a smoothing method – the inverse Fourier Fitting method – was developed. This method decomposes phenological information from a time series according to their frequencies and reconstructs time series by eliminating high-frequency components. The effectiveness of using different harmonics of this method has also been examined in this thesis.

In South Florida, hurricanes are common disturbances to the local ecosystem. During 2005, two major hurricanes – Hurricane Katrina on Aug. 25th and Hurricane Wilma on Oct. 24th – hit this region and consequently caused damage especially to mangroves, one of the most vulnerable vegetation types in this region

(www.nhc.noaa.gov). Several studies have evaluated the effects of hurricanes on vegetation, but few studies have examined the recovery rates of different types of vegetation after hurricanes.

The purpose of this thesis is to evaluate the use of NDVI time series with an 8-day interval derived from the Moderate Resolution Imaging Spectroradiometer (MODIS) Terra in order to detect the recovery rates of mangroves and other vegetation types following Hurricane Katrina and Wilma by using ordinary least square (OLS) method. The spatial recovery pattern is examined as well as a search for a spatial correlation between land-cover types and recovery rates. The results show that the fastest recovery rate occurred within the first year, and after two to three years, most of the vegetation returned to its pre-hurricane status. Similar recovery rates had been found within similar vegetation types, a finding that supports the efficacy of this method.

After a brief introduction, the literature on related studies is presented in Chapter 2. This chapter summarizes former landscape studies, NDVI principles, and vegetation damage and recovery studies in order to provide a theoretical background for the current thesis. The scientific insights gained from landscape studies and remotely sensed technologies in recent years are first outlined. This chapter also presents principles and theories related to NDVI in order to demonstrate its advantages for analyzing the vegetation information and their temporal behavior. NDVI data quality is also considered in this thesis. Several different ways of decreasing noise in NDVI time series are delineated to find a suitable noise reduction method. The properties of MODIS, the source of the NDVI time series, are also presented. Information about the study region – mangroves and other vegetation types

in the South Florida region – are then shown, as well as information about Hurricane Katrina and Wilma, which hit the South Florida region consecutively, approximately three months apart.

Chapter 3 illustrates the data and methodology used in this thesis. The satellite data derived from MODIS Terra were processed into a single NDVI time series and supplemental data – the mangrove data and the land cover map – are presented. The data smoothing method, the inverse Fourier Fitting method, is then introduced and applied to smooth this time series using different harmonic numbers. The principle of the OLS method and how it will be used for the NDVI time series is explained next. To summarize the results from OLS, the results are processed through the unsupervised classification method and compared with an existing land cover map.

Chapter 4 contains a discussion of the results from the previous chapters. The effectiveness of different harmonic numbers used to smooth the NDVI time series is shown and the efficacy of different numbers are compared using the coefficient of determination (r^2) and the root mean square error (RMSE). The OLS slope images are then illustrated with the information extracted from the whole study area, including the mangroves. The comparison between the unsupervised classified slope image of the recovery time period with the land-cover map is also displayed to show the spatial correlation between land-cover types and recovery rates. The results show that 16 harmonics produced the best fit and was therefore the most suitable for smoothing the NDVI time series analyzed in this thesis. The most intensive recovery time period was during the first year after hurricanes. In this study, similar recovery rates are detected within different land-cover types, a finding that provides good support for this method. These conclusions are drawn in the final chapter (5), as well as discussions for future work.

Chapter 2

Literature Review and Study Area

2.1 Literature Review

The interest in land cover analysis from local to global scales has attracted increasing attention since the late 1990s (Cihlar et al. 2000). Understanding and quantifying land changes processes is necessary to ensure a sustainable management of natural resources (Turner 1987). Analysis and characterization of land use and land-cover change are becoming necessary to understand and predict land-cover change processes. Traditional methods, such as field surveys, are labor intensive relative to remote sensing, which has emerged as the most useful data source for quantitatively measuring land-cover changes at the landscape and smaller scales with a relatively low expense (Petit et al. 2001). Through analysis of time series of remote sensing data, the dynamics of land-cover change processes may be investigated. Moreover, remote sensing has become an important source of information for monitoring vegetation conditions and land use or land-cover changes (Chu et al. 2009). Vegetation Index (VI) time series derived from satellite images are some of the most important sources of information in detecting vegetation conditions as well as in monitoring land cover processes.

The NDVI (Normalized Difference Vegetation Index) is one of the most widely used vegetation indices in recent years that measure and monitor plant growth, vegetation cover, and biomass production from multi-spectral satellite data. It is calculated from a normalized transformation of near-infrared (NIR) and red reflectance as follows:

$$NDVI = \frac{NIR - RED}{NIR + RED}$$

The principle behind NDVI is that chlorophyll causes considerable absorption of incident red light, whereas the spongy mesophyll leaf structure produces considerable reflectance from the near-infrared region of the spectrum (Tucker 1979; Giri et al. 2007; Hasegawa et al. 2009). As a result, high NDVI values will appear with vigorously growing healthy vegetation because of the low red-light reflectance and high near-infrared reflectance. This relatively simple transformation leads to output values ranging from -1.0 to 1.0. NDVI relates linearly to increasing leaf canopy density, which indicates increasing amounts of green vegetation. NDVI values near or less than zero relate to non-vegetated features like barren surfaces (rock and soil) and water, snow, ice, and clouds (USGS, http://ivm.cr.usgs.gov/whatndvi.php). Fig. 2.1 shows a global NDVI image that depicts the distribution of different land cover types.

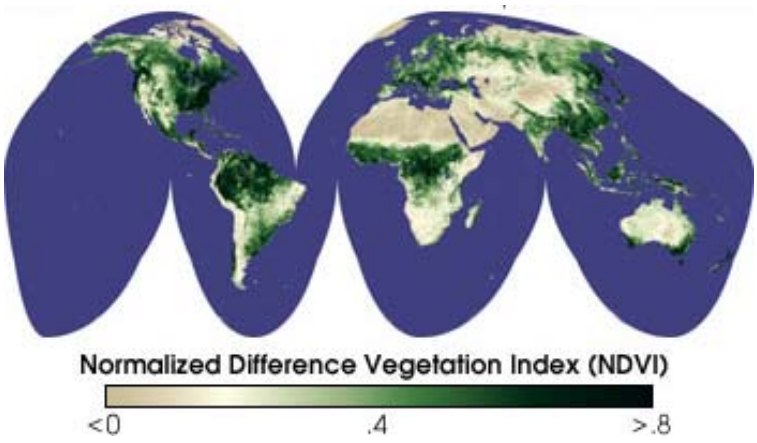

Fig. 2.1 An example of an NDVI image on September 21-30, 1999 for the global scale (From NASA website: http://earthobservatory.nasa.gov/Features/MeasuringVegetation/)

Large physical disturbances, such as fires, tropical cyclones (hurricanes or typhoons), tornados, ice storms, volcanic ash and landslides, can have major impacts on ecosystem structure and function; that is, such disturbances might induce significant changes in land-cover. The NDVI value indicates a level of photosynthetic activity despite varied levels of resilience among different vegetation species. Significant land-cover changes may result in NDVI value changes in areas affected by such disturbances: the comparison of one NDVI image of a period to an NDVI image of another period may be used to measure land-cover changes (Cakir et al. 2006). Therefore, a lot of studies have used NDVI to detect land-cover changes induced by various disturbances. For example, Rogers et al. (2009) examined the impact of Hurricane Katrina on Weeks Bay Reserve, Alabama. The images for March 2005 and September 2005 were compared. The comparison showed that during this time period, the average NDVI values decreased by 49% after landfall. The average NDVI values remained 44% lower in April 2006 compared with their values in March 2005 (Rodgers et al. 2009). Another study used NDVI to monitor the damage of mangroves in Phang Nga, Thailand after the 2004 Indian Ocean tsunami (Kamthonkiat et al. 2011). In van Leeuwen's 2008 study, phenological metrics – the start and end of the season, the base and peak NDVI, and the integrated seasonal NDVI extracted from NDVI time-series – were compared between burned and unburned areas to detect post-fire vegetation response in USA, Spain, and Israel (van Leeuwen 2008).

Besides the land-cover changes of the ecosystem induced by disturbances, the post-disturbance recovery patterns are also an important aspect of studying land-cover processes. It could provide us with a better understanding of vegetation recovery mechanisms. Time series data for NDVI may be derived from a variety of multispectral satellite systems such as NOAA/AVHRR (Advanced Very High

Resolution Radiometer), Terra or Aqua MODIS (Moderate Resolution Imaging Spectroradiometer), or SPOT/VEGETATION (SPOT/VGT) with slight differences in band ranges (see in Table 2.1) (Vrieling et al. 2011).

	AVHRR/3	SPOT/VGT	MODIS
Red (nm)	580-680	610-680	620-670
NIR (nm)	725-1,000	780-890	841-876

Table 2.1 Spectral characteristics (nm) of the red and NIR bands for different sensors

Among these sensors, the MODIS is a key instrument aboard the Terra (EOS AM) and Aqua (EOS PM) satellites. The orbit of Terra around the Earth passes from north to south across the equator in the morning, while Aqua passes from the opposite direction and crosses over the equator in the afternoon. For every 1 to 2 days, Terra MODIS and Aqua MODIS, acquire data in wavelengths from 0.4 μm to 14.4 μm and include 36 spectral bands to provide a view of the entire Earth's surface. MODIS is an important instrument in the development of global, interactive Earth system models, which support analyses of global changes that help policymakers formulate practical, suitable decisions about environmental protection. Patil et al. (2012) used MODIS spectral data to report the above ground biomass (AGB) of forests in the southern part of Gujarat state in India (Patil et al. 2012). Further, the Enhanced Vegetation Index (EVI) time series derived from MODIS was used to identify vulnerable areas in order to establish a soil erosion risk map in Tunisia (Kefi et al. 2012). Several different studies indicate the efficacy of using MODIS data in examining phenological problems.

Ideally, NDVI time series should show small changes with respect to a short time period, and thus an NDVI temporal profile should be continuous and smooth. However, cloud cover variation, data transmission errors, incomplete or inconsistent atmospheric correction, and bi-directional effects are all possible factors that result in frequent fluctuations in multi-temporal NDVI data sets. The influence of these factors has been discussed by several studies, namely that those effects could decrease the reliability of results (Los et al. 2000). There are several different preprocessing methods used to eliminate noise, including Maximum Value Composite (MVC). MVC is applied in order to obtain a higher percentage of clear-sky data, or brightness adjustment, such as the partial correlation for Rayleigh scattering (Verhoef et al. 1996; Ma et al. 2006; Tucker et al. 2001). However, simple preprocessing methods cannot necessarily remove all the influence and the residual noise left in time series and may impede further analysis, thus generating erroneous results (Chen et al. 2004). Therefore, some scientists have examined several methods for reducing noise levels and reconstituting higher-quality NDVI time series, such as the best index slope extraction (BISE) method, asymmetric Gaussian function fitting, or Fourier filter. Among the different data filtering methods, Fourier filter may be more suitable for vegetation recovery after disturbance studies because the method yields a smoother time-series than the other methods (Chen et al. 2004).

The Fourier filter has been applied in a variety of studies. For example, Sellers et al. (1994) used a series of adjustments to eliminate the errors in the NDVI continental data set caused from scattering, absorption of radiation in the atmosphere, and sensor degradation in order to generate global fields of terrestrial biophysical parameters. Also, a Fourier wave adjustment was first launched to adjust the problem of outliers (Sellers et al. 1994). The Fourier method was also used by Los et al. (2000) to build a

global nine-year biophysical land surface dataset using NDVI time series. This study found agreement between the estimated and observed data, and thus illustrated the effectiveness of this method (Los et al. 2000).

Various studies have used NDVI time series to detect recovery patterns after physical disturbances, especially fires. For example, van Leeuwen (2008) conducted a study using MODIS NDVI time series to monitor post-fire recovery in Arizona. Phenological metrics, such as the start and end of the season, the base and peak NDVI and so on, were extracted from NDVI time series as well. Pre-fire and post-fire trends and anomalies from different sites (burned and unburned) were evaluated by examining and computing the post-fire seasonal trends in NDVI of the long-term seasonal average time-series data. These trends were then assessed through analysis of the seasonal differences between average NDVI values for each year. Additionally, MODIS time-series NDVI data were summarized for each of the burned and referenced sites by calculating the eleven phenological metrics for each year (van Leeuwen 2008). In another study Goetz et al. (2006) used AVHRR NDVI time series to analyze fire disturbance and forest recovery across Canada and found that the anomaly differences, which represent residual variations, illustrated significantly reduced NDVI during the time of fire. Comparison between burned and unburned sites led to the conclusion that it took less than five years to reach recovery to the pre-burn level (Goetz et al. 2006). Further, Kamthonkiat et al. (2011) used NDVI time series derived from Advanced Spaceborne Thermal Emission and Reflection Radiometer (ASTER) images to compare areas of mangrove coverage from different dates. Then NDVI curves were used to observe recovery patterns after the 2004 Indian Ocean tsunami in Phang Nga, Thailand (Kamthonkiat et al. 2011).

Other studies have used different vegetation indices to detect recovery patterns. Wittenberg et al. (2007) used the Enhanced Vegetation Index (EVI) instead of NDVI time series to analyze the spatial as well as temporal recovery patterns of vegetation in a Mediterranean landscape after the sequences of forest fires. Multivariate analysis of variance (MANOVA) was used to analyze the influence of different factor (like aspects and climate variables) on post-fire vegetation recovery time period. The author concluded that vegetation would recover back to the pre-disturbance level within five years following a single fire. Further decrease of EVI values might appear after repeated fires, and the detected trend was more pronounced on south-facing slopes (SFS) than north-facing slopes (NFS) (Wittenberg et al. 2007).

Mangroves are a special type of wetland that consists of medium height trees (ranging from 6 m to 30 m) and shrubs growing in coastal habitats in the tropics and subtropics areas. The environmental and socioeconomic values of mangroves are well known. Mangroves occupy 137,760 km² of coastal areas worldwide (Rocchio, 2010) (Fig. 2.2) and provide several important functions that include supporting diverse food webs, assisting with water quality improvement, and protecting coastlines against tropical storm surges. Mangroves may provide economic values up to $200,000–$900,000 US dollars per hectare (Wells 2006) and benefit coastal inhabitants directly and indirectly as a source of fuel, medicine and supplementary food (Giri et al. 2007). Despite the importance of mangroves, they are among the most vulnerable vegetation types affected by disturbances and environmental changes, such as those resulting from hurricane and tsunamis. Studies have shown that mangroves tend to bear most of the damage from hurricanes and tropical storms (Piou et al. 2006; Krauss et al. 2005). For example, Omo-Irabor (2011) built a mangrove vulnerability model using satellite images, GIS techniques and spatial multi-criteria

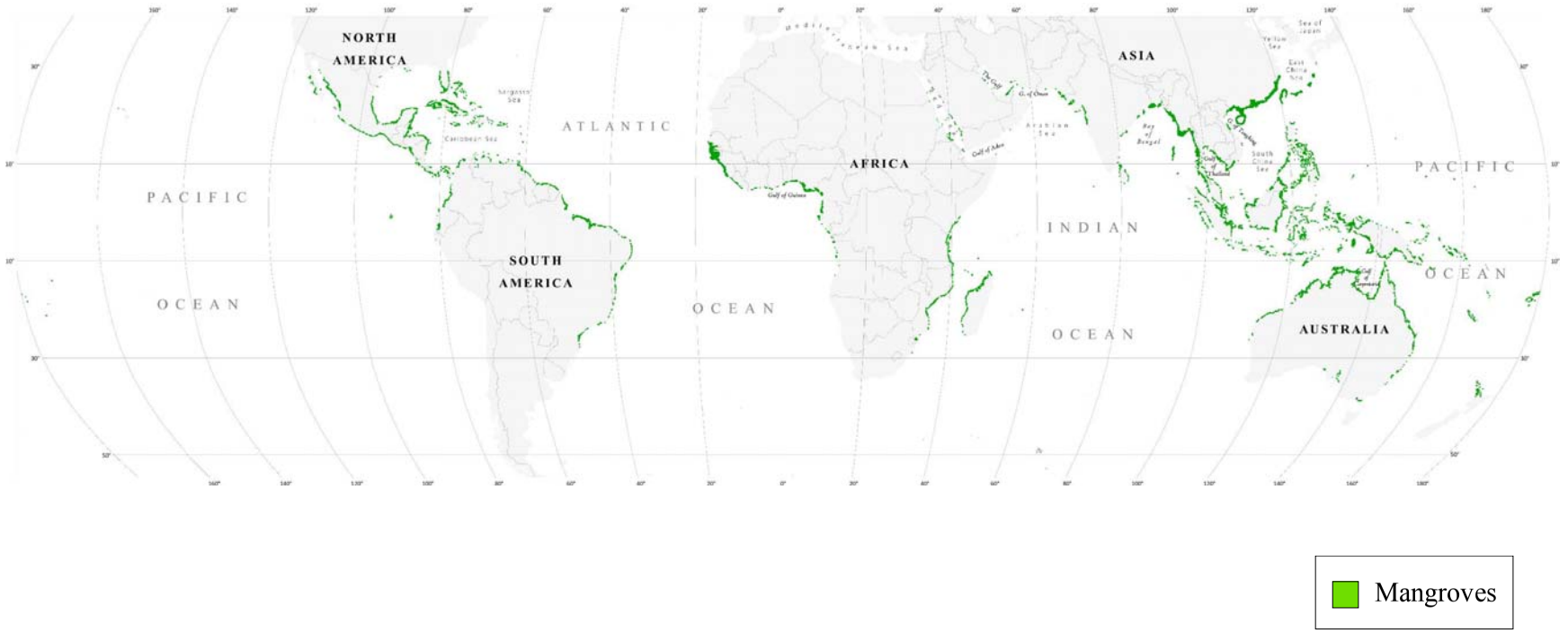

Fig. 2.2 Worldwide mangrove distribution in 2010 Created from Landsat data by USGS-EROS group led by Chandra Giri (http://landsat.gsfc.nasa.gov/graphics/news/sci0030lg.jpg)

analysis (SMCA) in parts of Western Niger Delta, Nigeria (Omo-Irabor et al. 2011). Further, Piou (2006) studied the zoning patterns of 41 years for mangrove forests in offshore Belize following a catastrophic hurricane (Piou et al. 2006).

The largest mangrove ecosystem in the western hemisphere is located in Everglades National Park within the South Florida region. Everglades National Park is not only a large (around 6,100 km^2) sub-tropical wetland, but also contains ridges with dense vegetation, relatively open sloughs, and tear-shaped tree islands. It is the largest subtropical wilderness in the United States. More than 350 species of birds, 300 species of fresh and saltwater fish, 40 species of mammals, and 50 species of reptiles live within Everglades National Park (http://www.nps.gov/ever/index.htm).

In 2005, the South Florida region was affected by two major hurricanes – Hurricane Katrina and Hurricane Wilma. After these two hurricanes, intensive damage was observed over a widespread area, especially for the coastal mangrove ecosystems in Everglades (See Fig. 2.3).

Fig. 2.3 Hurricane effect in Everglades National Park, comparison of before and after (T. J. Smith III, 2007)

Many studies have analyzed Hurricane Katrina's and Hurricane Wilma's impacts on mangrove forests in this region. For example, Doyle et al. (2009) used airborne videography to analyze landscape patterns of the hurricanes' impact as well as wind circulation in mangrove forests of the Everglades. Two aerial video transects, representing different topographic positions were used to quantify forest damage from video frame analysis in relation to prevailing wind force, tree-fall direction, and forest height. A hurricane simulation model was applied to reconstruct wind fields corresponding to the ground location of each video frame and to correlate observed tree-fall and destruction patterns with wind speed and direction. The conclusion from this analysis was that the mangrove area suffered whole or partial blow-downs within the storm's eye-path and the right-side (fore-wind) quadrants, whereas left-side (backwind) sites south of the eye-wall zone incurred moderate canopy reduction and defoliation (Doyle et al. 2009). Other studies have analyzed different aspects of the hurricanes' impact on mangrove forests, such as Castaneda-Moya et al. (2011), who quantified sediment deposition and nutrient inputs in Florida Coastal Everglades (FCE) mangrove forests related to this storm event. The magnitude of fluxes that regulate nutrient biogeochemistry in mangrove forests of South Florida were also evaluated (Castaneda-Moya et al. 2011).

Besides mangroves, several different vegetation types within the South Florida region also suffered damage from hurricanes. For example, Cushman et al. (2006) studied the yields of tomato crops after Hurricane Wilma in order to estimate the wind damage on crops in southern Florida (Cushman et al. 2006). Another study examined the effect of Hurricane Andrew on fruit crops and concluded that older and taller

trees were more severely damaged than younger and shorter trees. Moreover, this study also summarized the different responses from different crop species (Campbell et al. 1993).

Despite previous studies that have examined the impact of hurricanes in this region, relatively few have analyzed the rates of recovery from these disturbances of mangrove forests and other vegetation types by using a time series of NDVI from the MODIS Terra satellite. In the current thesis, this gap will be addressed by using the smoothed time-series to detect mangrove and other vegetation types' recovery patterns after the major disturbances of Hurricane Katrina and Hurricane Wilma in 2005 in South Florida, south from Lake Okeechobee.

To this end, the Ordinary Least Squares (OLS) method will be used in this thesis to map recovery trends. The OLS method has been used in different studies. Climate data and remote sensing data were used to evaluate alpha diversity estimates through this method in tropical rain forests of West Africa and Atlantic Central Africa (Parmentier et al. 2011). In another study, OLS regression had been used to examine the interdependence between spectral heterogeneity and net primary production (NPP) proxies, such as NDVI (Rocchini et al. 2010). This kind of method has also been used to detect trends in NDVI. For example, Fuller (1998) used this linear method to detect trends in NDVI time series in order to estimate their relation to rangeland and crop production in Senegal (Fuller 1998).

2.2 Study Area

The South Florida region is defined in this study as the region south of Lake Okeechobee (Fig 2.4). This map is created using the NASA Blue Marble: Next Generation 500m resolution imagery from ArcGIS 10 base-map

(http://earthobservatory.nasa.gov/Features/BlueMarble/). The study area is an approximately 64,100 km^2 area of land in 16 counties. The land cover of the region is diverse and includes not only Everglades, Water Conservation Areas, Big Cypress National Park, water bodies such as Lake Okeechobee and Caloosahatchee River but also a most highly urbanized area consisting of Palm Beach, Broward, and Miami-Dade counties. These counties contain 30 percent of Florida's residents (http://www.census.gov/).

The South Florida Ecosystem is an important reservoir of landscape, community, and species diversity (Brook 1974). The vegetation of South Florida represents a mixture of Caribbean, southern temperate, and local influences. As a result of this convergence of Caribbean, temperate, and endemic influences, the South Florida Ecosystem – comprising the only subtropical ecological communities in the continental United States – supports substantial ecological, community, taxonomic, and genetic diversity (http://www.fws.gov/).

All these features make this area an important and unique region to study and protect, but Florida is constantly under threat of hurricane disturbance, which could cause a lot of damage in this ecosystem. During 2005, two major hurricanes hit this South Florida region. On 25 August, 2005, Hurricane Katrina made its first landfall in the United States to the east of the Everglades as a category 1 (119-153 $km \cdot hr^{-1}$) hurricane with maximum sustained winds of 130 km, and soon degraded to a tropical storm (slower than 118$km \cdot hr^{-1}$) after crossing Florida. In contrast to Hurricane Katrina, Hurricane Wilma approached southwestern Florida from the Gulf of Mexico and made landfall on 24 October 2005 with maximum sustained winds of 195 $km \cdot hr^{-1}$ (category 3) (178 $km \cdot hr^{-1}$ - 209 $km \cdot hr^{-1}$), which was stronger and caused more damage than Hurricane Katrina in this region (http://www.nhc.noaa.gov/). The

hurricane tracks are shown in Fig. 2.4. Although the damage caused by these two hurricanes was irreversible to this unique ecosystem, it made this area a suitable example to study hurricane damage on vegetation and subsequent vegetation recovery rates.

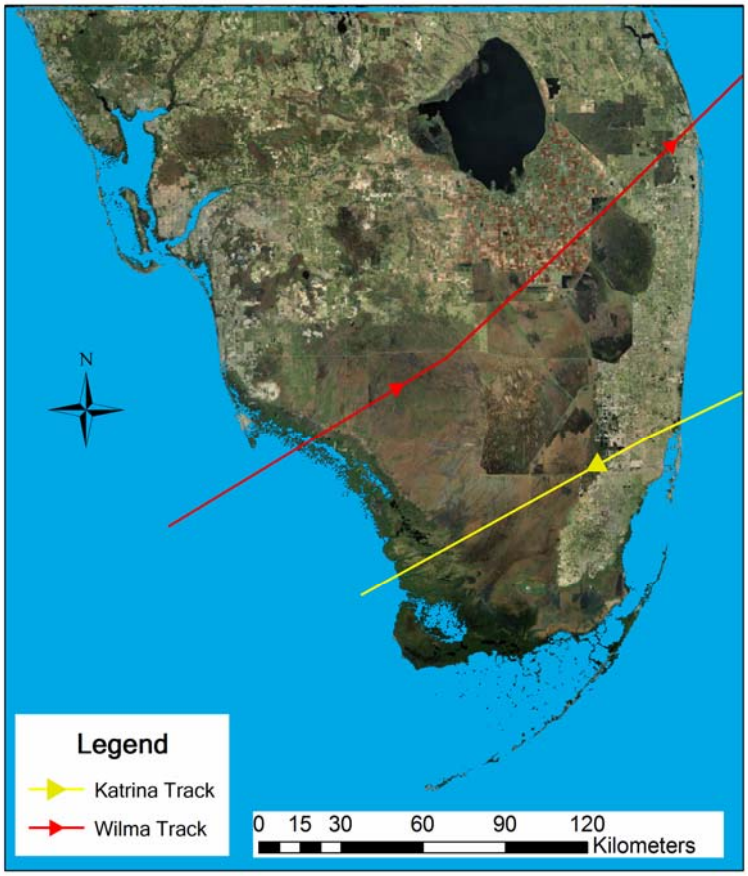

Fig. 2.4 Satellite imagery from MODIS of study area with tracks of Hurricane Wilma and Katrina

There are various land-cover types in this region such as beach dune, coastal strand, hardwood hammocks, rock-land pine forests, scrub, wet prairie, mangrove and cypress swamps, coastal salt and freshwater marsh, sloughs (Myers et al. 1990; (Duever et al. 1986). To better analyze different land-cover types, the classification scheme of the Global Land Cover 2000 Project (GLC 2000) (http://bioval.jrc.ec.europa.eu/products/glc2000/glc2000.php), which used the VEGA

2000 dataset to create a land-cover map for the whole world, were utilized in this thesis; according to this project, there are 16 different land-cover types in the South Florida region (Fig. 2.5).

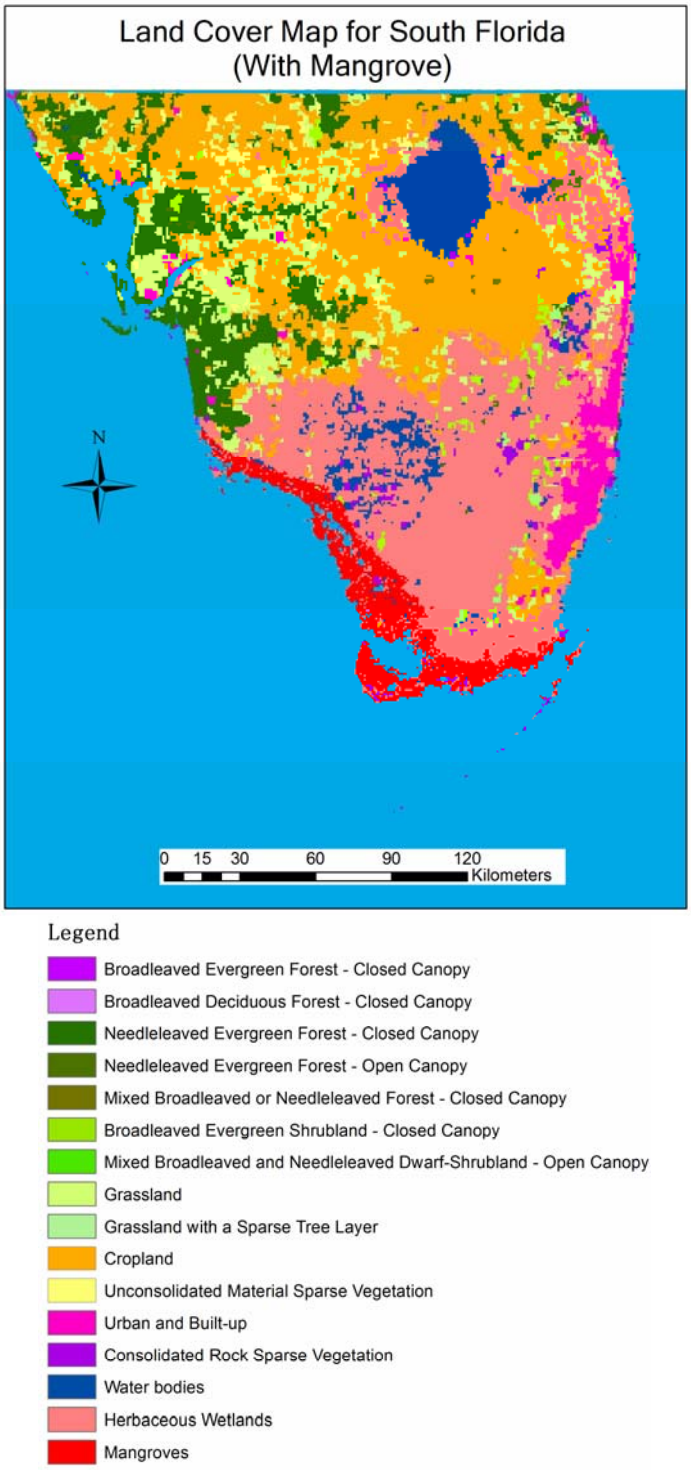

Fig 2.5 Land cover map for study area
(http://bioval.jrc.ec.europa.eu/products/glc2000/glc2000.php)

Chapter 3

Data and Methodology

3.1. Data

3.1.1 Satellite Data

In this thesis, NDVI time series was formed by 8-day interval images from 2001 to 2010, with 46 images for each year derived from MODIS Terra and calculated using band 1 (red) and band 2 (NIR). The spatial resolution is 250 m. The MODIS 8-day images are maximum value composite (MVC) product, which means that for every cell in the image, the highest value during each 8-day period, is retained to create each image in the series, which reduces the effect of clouds, aerosols and water vapor. One image was missing in the time series (22^{nd} in the sequence centered on Jun. 18th 2001). The missing data was filled by averaging the images before and after the missing composite. Fig. 3.1 shows the mean NDVI for South Florida from 2001 to 2004.

3.1.2 Mangrove Data

The mangrove area in South Florida covers approximately 1,600 km^2 and is distributed mostly in southwestern costal region (Fig. 3.2). In the southeastern part of the Everglades, the dominant species is red mangrove, existing in scrub and dwarf forms and reaching 2.5 m in height. In the southwest and along fringes of the numerous islands in and around Florida Bay, red mangroves occur in a taller form, reaching 19 m at maturity in dense stands (Barr et al. 2009). The mangrove mask (Fig 3.2) was used to extract mangrove slope values.

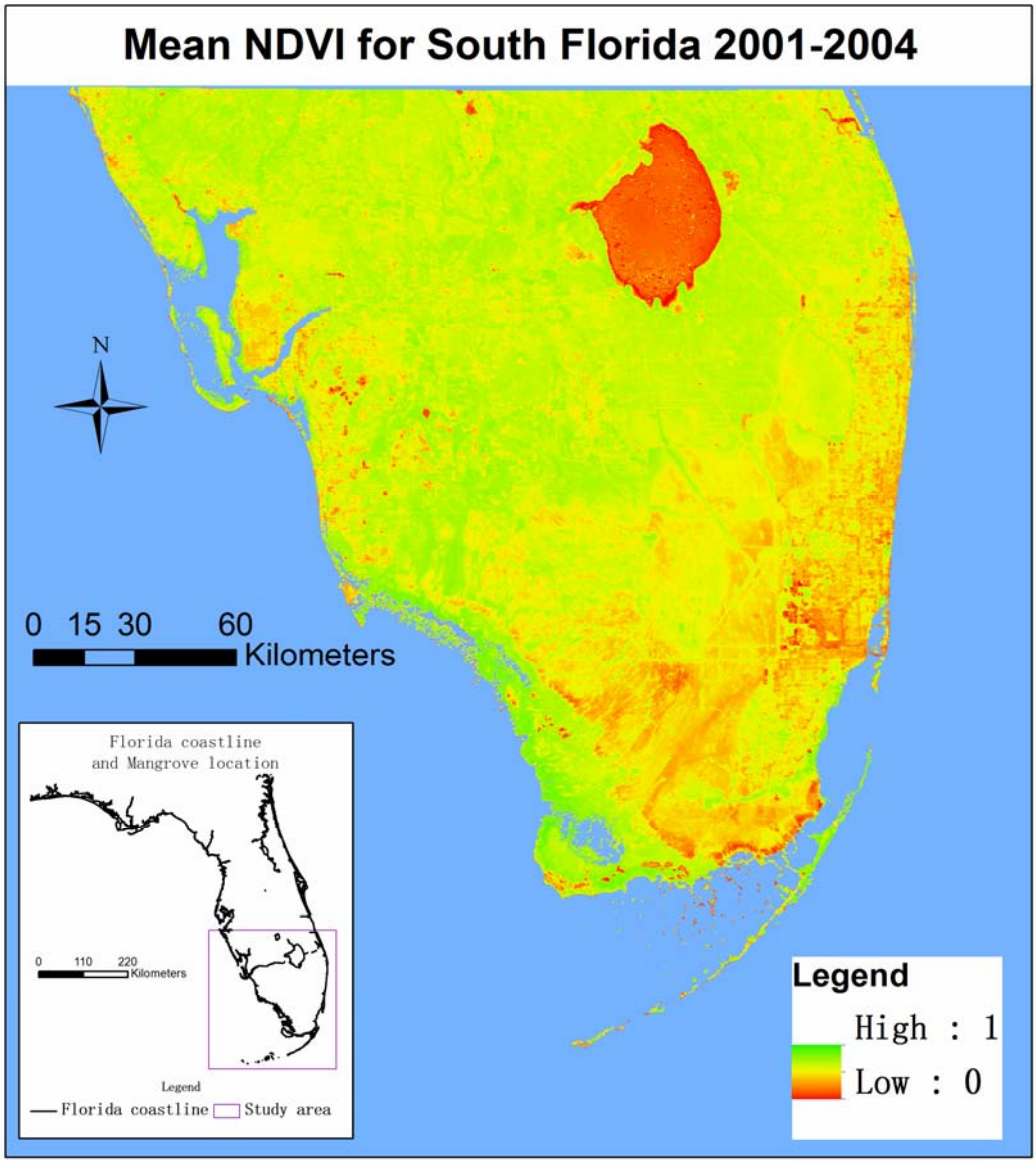

Fig. 3.1 The mean NDVI for South Florida from 2001 to 2004

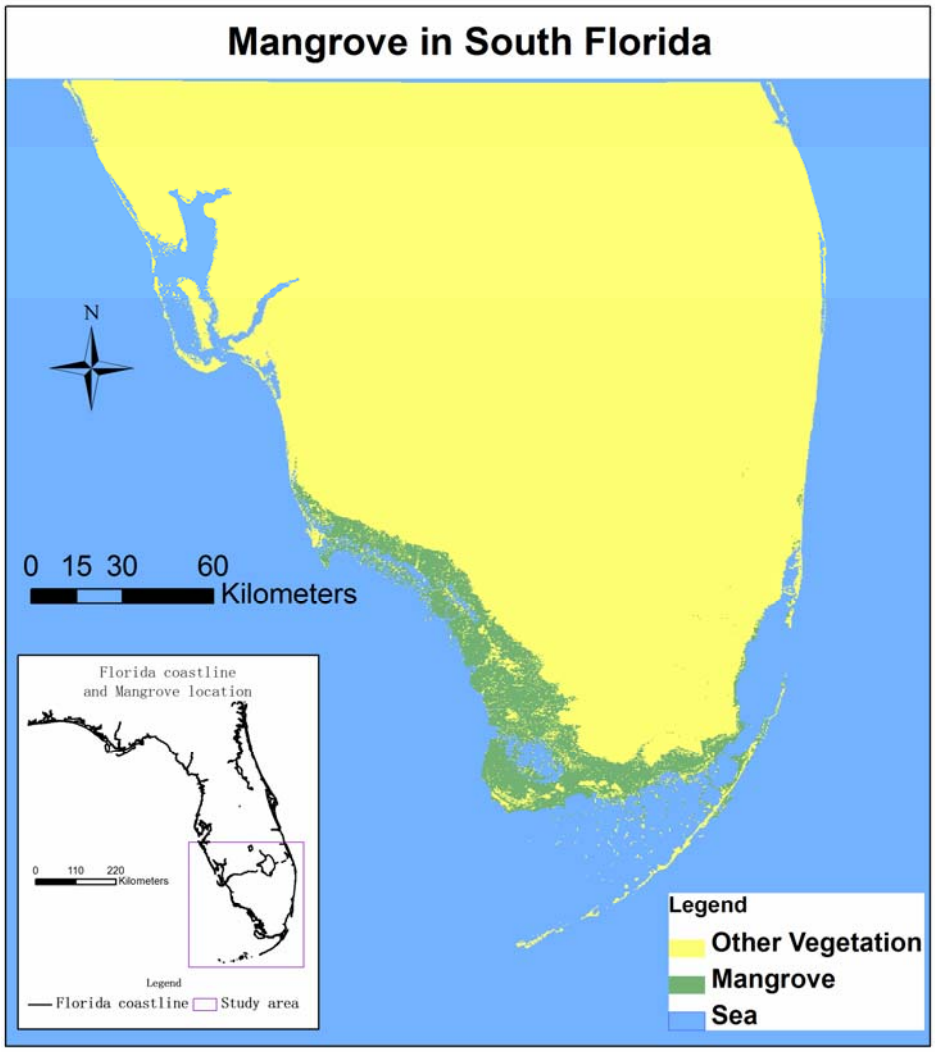

Fig. 3.2 Mangrove mask in South Florida
(ftp://sfnrc.net)

3.2 Data Smoothing

Although the MODIS 8-day products are MVC processed which helps reduce or eliminate clouds from a scene, frequent fluctuations caused by other factors could remain. An inverse Fourier de-noise method was used because the Fourier-based fitting methods are suitable for all kinds of studies and can result in a smoother curve

for further analysis than other methods such as threshold or asymmetric function fitting method (Chen et al. 2004). The Fourier transformation is a mathematical operation that decomposes a function into different sinusoidal components with different frequencies. The procedure of an inverse Fast Fourier transformation was applied as follow: first, the phenological information from the time series was decomposed into a series of sinusoids of different frequencies according to a Fourier transformation; second, proper reconstruction of the phenological signals was achieved through the inverse Fourier transformation utilizing different numbers of components decomposed from the first step, which is called harmonics as well (Jakubauskas et al. 2001). Previous studies have indicated that 50–90% of the variability in a time series could be maintained using the first two harmonics when utilizing the inverse Fourier transformation, but the first two harmonics can only be used to display annual and semi-annual cycles. Consideration of the first four harmonics reveals natural phenological cycles (Geerken et al. 2005; Jeganathan et al. 2010), although these studies utilized this method on a time series one year in duration. According to the technical literature, the number of the harmonics should be based on the length of the series as well (Page 174, Chapter Earth Trends Modeler, Idrisi Taiga Manual book). A value that works well is to include all the inter-annual cycles, including the annual and semi-annual cycles, which will double the number of years included (Page 174, Chapter Earth Trends Modeler, Idrisi Taiga Manual book). In the current thesis, 10 years of data were used, so the harmonic number should not be larger than 20. Several different numbers of harmonics – 8, 10, 12, 16, and 20 – were used to de-noise the time series in order to illustrate the effects of different harmonic numbers, and the data for mangroves were extracted separately from each smoothed result by using the mangrove mask previously provided. The several

smoothed time series were then compared with the raw data of mangroves individually using linear regression to determine the coefficient of determination (r^2) and the root mean square error (RMSE) in order to find out the best fit for further use.

3.3 Methodology

3.3.1 OLS slope analysis

The OLS was used to estimate the unknown parameters in a linear regression model. The relationship can be expressed by a simple linear equation. Suppose the data consists of n observations $(y_i, x_i)\ n_{i=1}$. Each observation includes a response y_i and a regressor x_i. In a linear regression model, the response variable is a linear function of the regressor shown as below, where the *b* is the slope value and *a* is the intercept value:

$$Y= bx + a$$

The OLS was used to express the linear relationship between time (the regressor variable) and NDVI (the response variable). The linear trend (OLS) function from the analysis tab in the Idrisi Taiga's Earth Trend Modeler is the function that calculates the slope coefficient of an OLS regression between the values of each pixel over time and a perfectly linear series. The result is an expression of the rate of change over a set of time steps. Thus, the analysis expresses the average rate of change per 8 days for the length of each input time series. In this way, the slope values could be regarded as recovery rates.

The phenology of vegetation in South Florida can be divided into two parts, the dry season from November – May, and the wet season from June - October. At the beginning of the wet season, the vegetation starts to grow and the NDVI starts to increase, which results in a positive value of the slope ($b>0$). At the start of the dry

season, photosynthetic activity begins to decrease, which results in a negative value of the slope ($b<0$). So for an annual cycle, the average slope value will be around zero ($b=0$). A major disturbance, such as a hurricane, may produce different levels of damage to plant canopies ranging from defoliation to complete destruction and large-scale mortality. A recovery period is expected during the time that photosynthetic activity appears to increase, which leads to a positive *b* value of the slope.

The NDVI time series is divided into three multi-year periods, pre-hurricane, recovery, and post-recovery. Each period covers a whole number of years in order to eliminate seasonal variation. In dividing the time series, the pre-hurricane periods includes the four years' NDVI image before Hurricane Wilma (10/31/2001 to 10/24/2005, 184 images). One-year (10/31/2005 to 10/24/2006, 46 images), two-year (10/31/2005 to 10/24/2007, 92 images) and three-year (10/31/2005 to 10/24/2008, 138 images) time periods after Hurricane Wilma were taken into consideration to examine the different rates of recovery within different time spans. The other post-hurricane periods (five-year period 10/31/2005 to 10/24/2010, 230 images) were considered post-recovery periods accordingly (Fig. 3.3). In this way, the effects from both Hurricane Wilma and Hurricane Katrina could be measured within the recovery periods. Separation of the time series into different parts could provide a clear comparison between pre-hurricane period and post-hurricane period to illustrate the recovery rate during the post-hurricane period. Moreover, by examining the different time period lengths, such as one year, two years and three years after hurricanes, different recovery rates with different time periods should better reveal the recovery pattern through time

The separated time series parts were processed using the linear model (OLS) function respectively to obtain the slope value images and to illustrate the spatial distribution of recovery rate. The slope value distribution of the study area was extracted to show the trend through time, and the mangroves data was extracted by calculating the mean values of all pixels in the mangrove mask shown in Fig. 3.3 to analyze the recovery rate for mangroves separately.

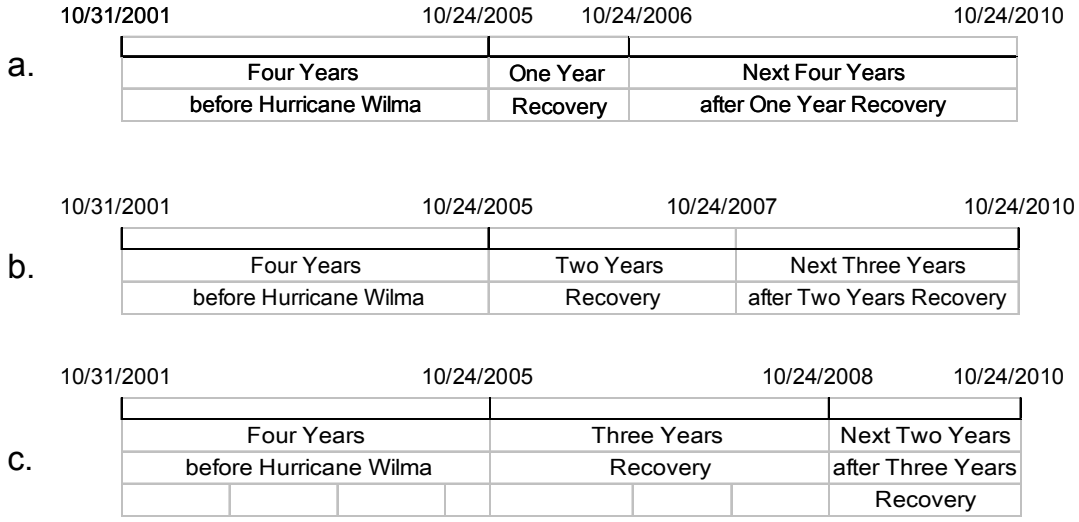

Fig. 3.3 Different ways NDVI time series were divided (a. one year after Hurricane Wilma recovery time period; b. using two years after Hurricane Wilma recovery time period; c. using three years after Hurricane Wilma recovery time period)

3.3.2 Unsupervised classification

Unsupervised classification was used to identify spectrally or temporally similar clusters in satellite imagery. It enables one to specify parameters, such as vegetation indices or band information, which the computer uses to uncover statistical patterns

that are inherent in the data. In the current thesis, the spatial patterns of recovery rate images were unknown, so the unsupervised classification was considered more suitable than a supervised classification.

The OLS regression slope images were produced as a set of raster images, each for one time period accordingly, with different values in each pixel. A layer stack was built to incorporate each recovery rate image into a single file, with each layer analogous to a different spectral band. The layer stack consisted of three images for the three recovery periods and was divided into five classes using ERDAS IMAGINE 2010.

3.3.3 Comparison

The classified image of the three recovery periods was compared with the re-classified land-cover map to see if they revealed spatial coherence or general qualitative agreement. The classified recovery rate image of the recovery period has a different spatial resolution (250 m) than the land-cover map (1000 m), so the recovery rate map was re-sampled to 1000m resolution to match the land-cover map. The re-sampled classified recovery rate image was then compared with the land-cover map, using the matrix function in ERDAS IMAGINE 2010. This function creates a cross-tabulation between the land-cover map and the reclassified recovery rate image. Each number in the table represents the quantitative agreement between these two maps, which shows how many pixels belong to both a certain land-cover type and a certain recovery rate class. Using the total number of pixels for each land-cover type, percentages were calculated for each recovery rate class.

Chapter 4

Results

4.1. Smoothed NDVI Time Series

The NDVI data of the mangroves was extracted and is shown in Fig. 4.1, including the mean value and the standard deviation for the mangrove area. The annual cycle showing the seasonal variation can be seen as the single annual peak and minimum value within each cycle. The standard deviation is illustrated here as well, which shows how much spatial variation exists in each image. In this figure, low values frequently appeared with the peak of NDVI, which indicates that the data points tend to be very close to the area mean, whereas high standard deviation appeared around the bottom values, indicating that the data points are spread out over a large range of values.

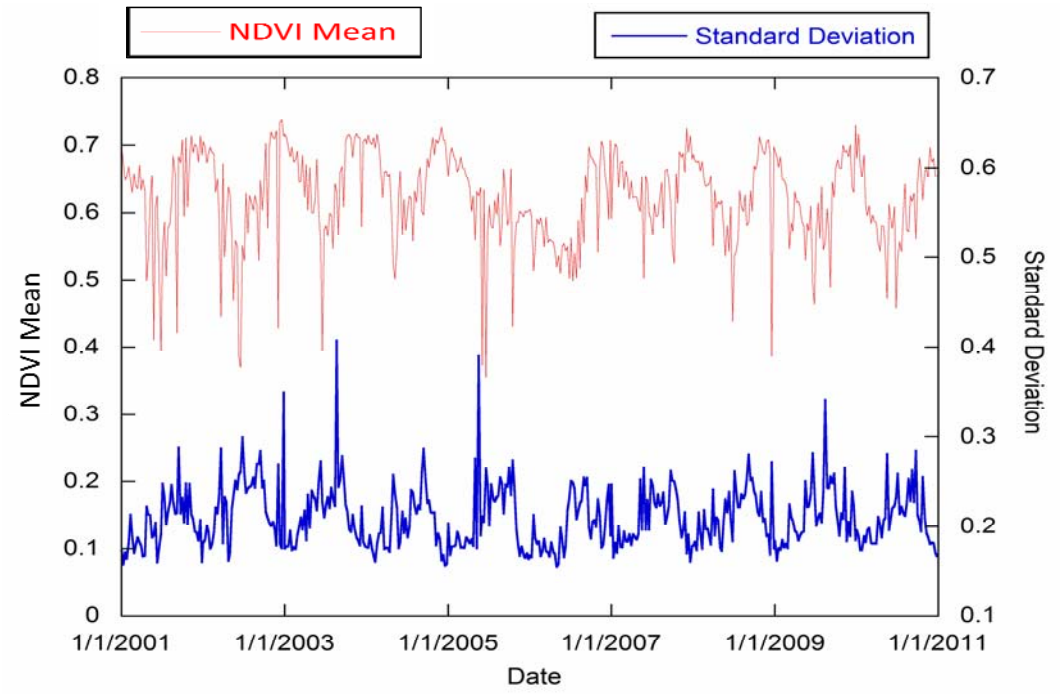

Fig. 4.1 The mean and standard deviation of NDVI value for mangroves shown in Fig. 3.2

The raw NDVI time series data (Fig. 4.1) displayed high-frequency noise, likely attributable to residual clouds or other effects, over the whole time series. To eliminate the influence of the noise, different numbers of inverse Fourier harmonics (8, 10, 12, 16 and 20) were applied in order to smooth the raw NDVI time series. The different harmonics produced distinct de-noise effects. The plots showing mean NDVI of mangroves between smoothed data and raw data are shown in Fig. 4.2. From these plots, it can be seen that the method resulted in different smoothed curves. For the eight-harmonic result the curve is smoothed, but the annual cycle and seasonal variance were not clear in this time series. The fitting level with the raw data also seemed low compared to the other numbers of harmonics: it increased commensurate with the increase in numbers of harmonics. The results from linear regression between the raw data and smoothed data (Table. 4.1) better illustrate the correlation between different numbers of harmonics with raw time series. The coefficient of determination (r^2) and the RMSE were derived from linear regression; the former indicates the level of fitting between the raw and smoothed data expressed in NDVI time series while the latter reveals the level of difference. The table clearly shows that the result from the eight harmonics had the lowest coefficient of determination of 0.11 as well as the highest root mean square error of 0.646. The coefficient of determination increased commensurate with the number of harmonics up to 16 harmonics (0.51) and then decreased with 20 harmonics (0.50). For the root mean square, the smoothed data with 16 harmonics had the lowest value, indicating less difference between the smoothed and raw data than the other fits.

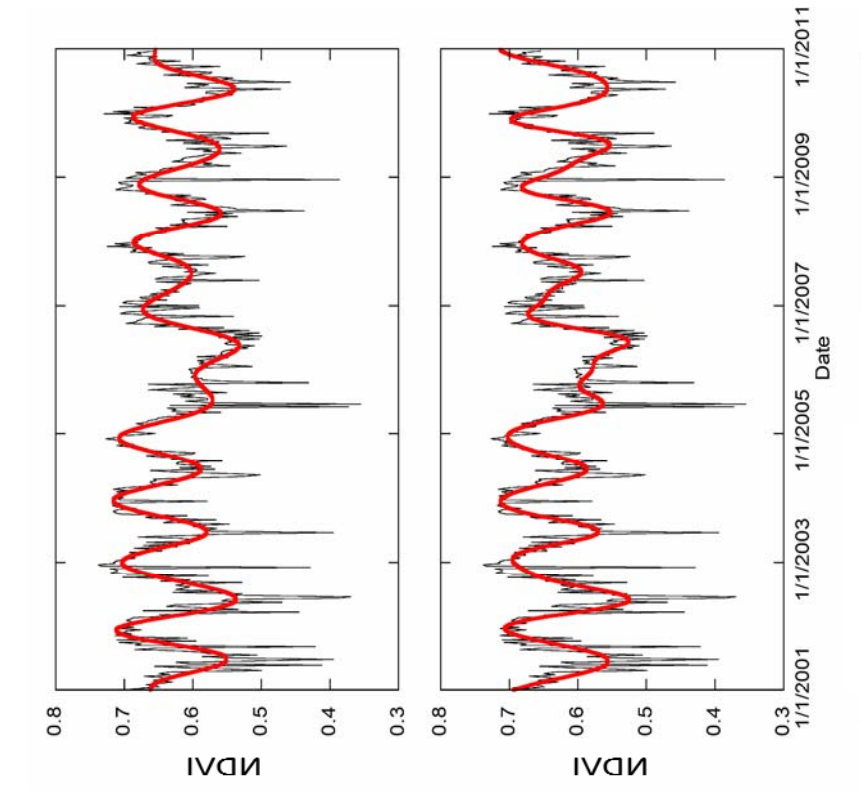

Fig. 4.2 Comparison between smoothed data of different harmonics with raw data of extraction from mangrove: (a) 8 harmonics; (b) 10 harmonics; (c) 12 harmonics; (d) 16 harmonics; (e) 20 harmonics.

	Coefficient of determination r^2	Root mean square error (RMSE)
8 harmonics	0.1126	0.0647
10 harmonics	0.4757	0.0504
12 harmonics	0.4951	0.0498
16 harmonics	0.5125	0.0478
20 harmonics	0.5067	0.0486

Table 4.1 Summary of the results of the linear regression

The resultant series smoothed using 16 harmonics were used to calculate the OLS slope images in the next step of the analysis. According to some previous studies (Geerken et al. 2009; Jeganathan et al. 2010), the most suitable harmonic number for the inverse Fourier filter method should be 3 to 5 for an annual time series. Results have shown that for multi-year time series, the harmonic number should be increased when the length of a time series is longer than one year.

4.2 OLS Slope Analysis

The results of Ordinary Least Square (OLS) slope images processed from 16-harmonic smoothed NDVI time series were a set of continuous images, with a unique value for each pixel. Each image showed the slope values, which represent the trend of each of the different time segments of the NDVI time series. The results are

shown in Fig. 4.3, Fig. 4.4 and Fig. 4.5 with different length of time series to represent different recovery periods for the whole study area, along with the pre-hurricane image (the same in all the three figures) and the post-recovery images for comparison. To better illustrate the results, all the maps' ranges were standardized to a range of -0.003 to 0.003, representing the rate of change in NDVI per 8-day period.

In these figures, the slope image of the period one year after the hurricanes displayed more positive values (b>0) (shown in red region) than the other two, which indicated a more widespread region of high recovery rate in the whole South Florida area (shown in Fig. 4.3). The area of positive values decreased along with the increase of the length of the recovery time, which indicates that some regions' recovery rates slowed within two years (shown in Fig. 4.4). Moreover, after three years of Hurricane Wilma, the positive value area was only a quite small portion (shown in red portion), which indicates that after three years' recovery, most of the study area had recovered to the pre-hurricane levels (shown in Fig. 4.5). To better illustrate these results, the frequency distribution for different recovery periods are shown in Fig 4.6 with a class width of 0.001 and total range from -0.01 to 0.01 (including 98% of the first-year pixels and more than 99% for both two- and three-year time series).

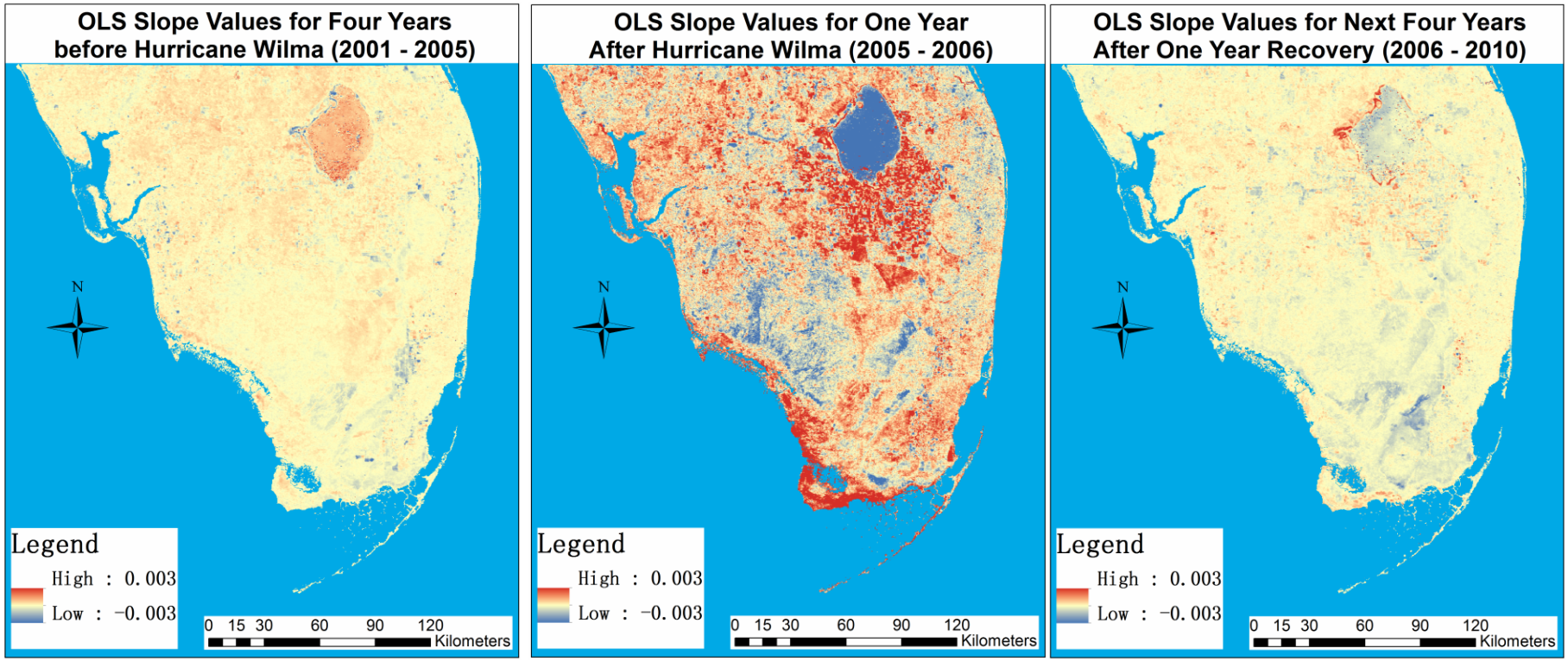

(a) (b) (c)

Fig. 4.3 Images for OLS slope values: (a) Pre-Hurricane period from 2001-10-31 to 2005-10-24; (b) One year after Hurricane Wilma from 2005-10-31 to 2006-10-24 (c) The time period from 2006-10-31 to 2010-10-24

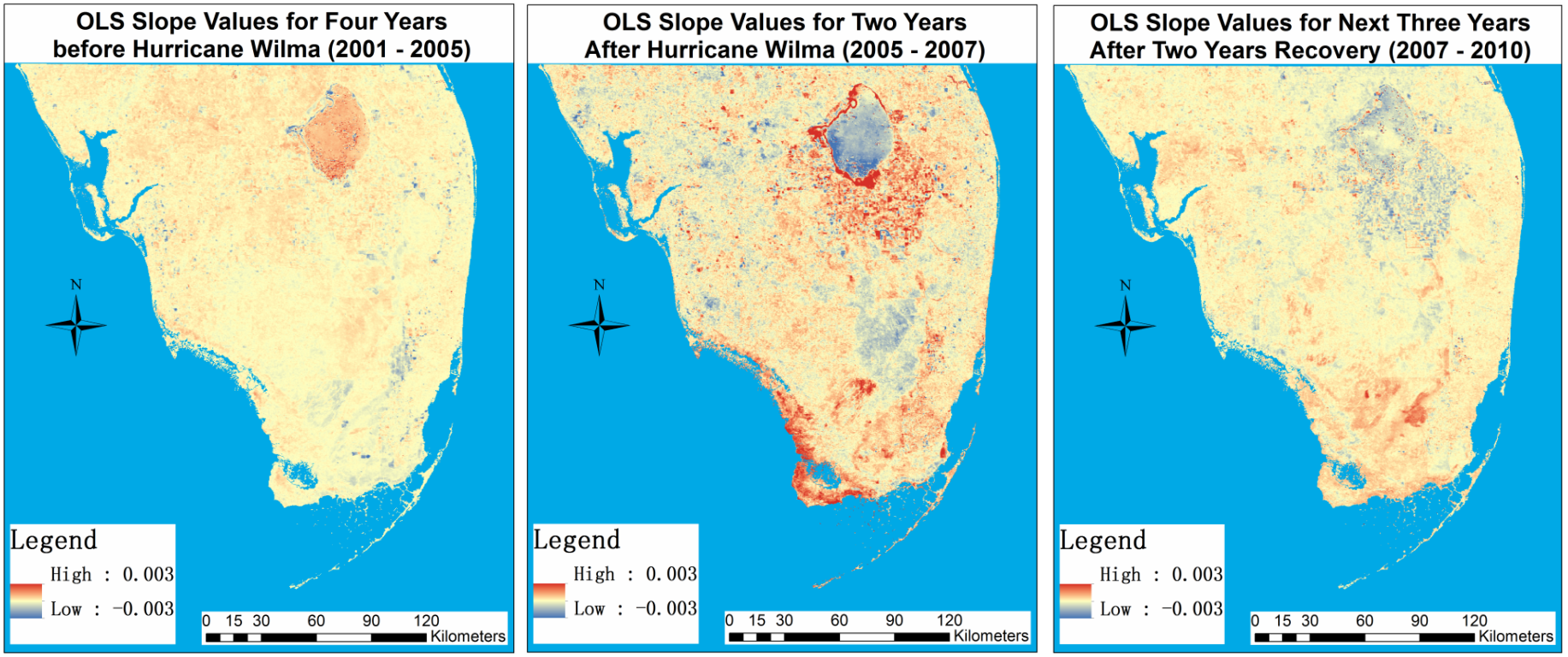

(a) (b) (c)

Fig. 4.4 Images for OLS slope values: (a) Pre-Hurricane period from 2001-10-31 to 2005-10-24; (b) Two years after Hurricane Wilma from 2005-10-31 to 2007-10-24 (c) The time period from 2007-10-31 to 2010-10-24

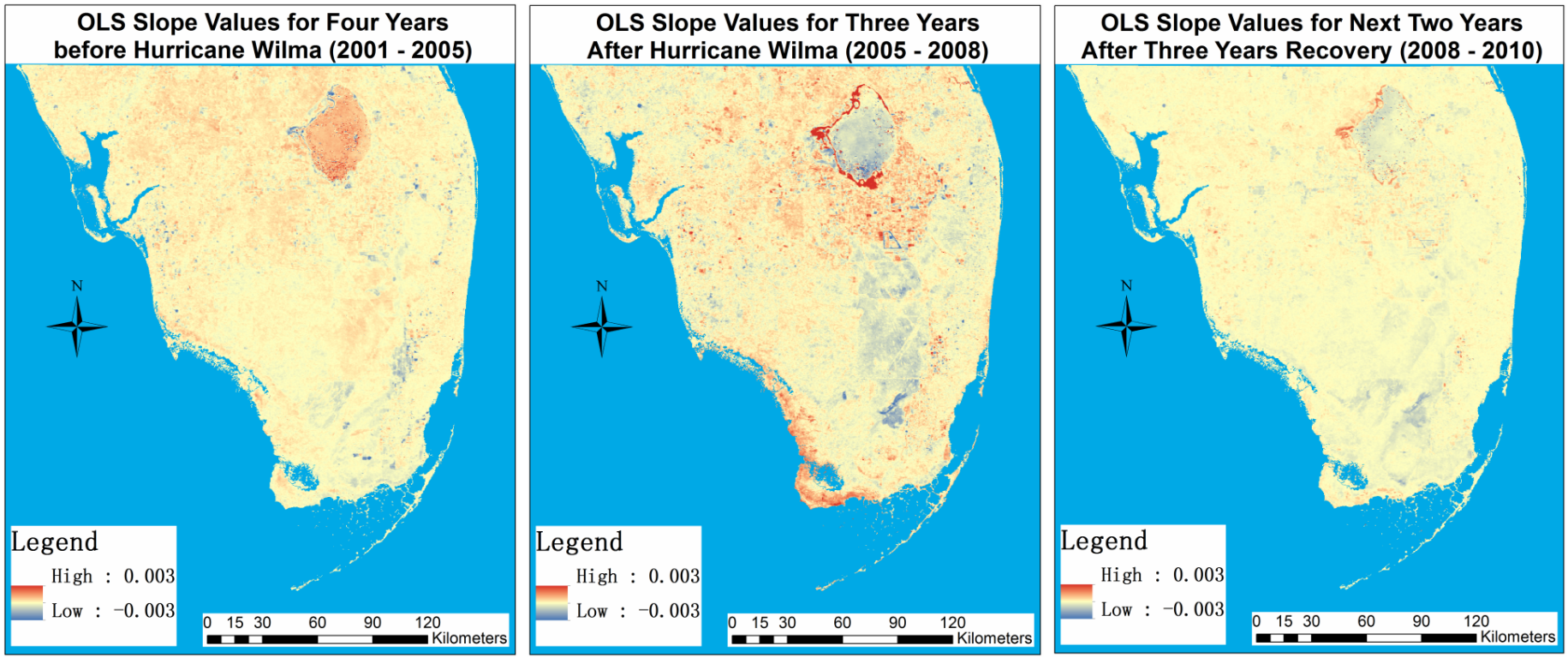

(a) (b) (c)

Fig. 4.5 Images for OLS slope values: (a) Pre-Hurricane period from 2001-10-31 to 2005-10-24; (b) Three years after Hurricane Wilma from 2005-10-31 to 2008-10-24 (c) The time period from 2008-10-31 to 2010-10-24

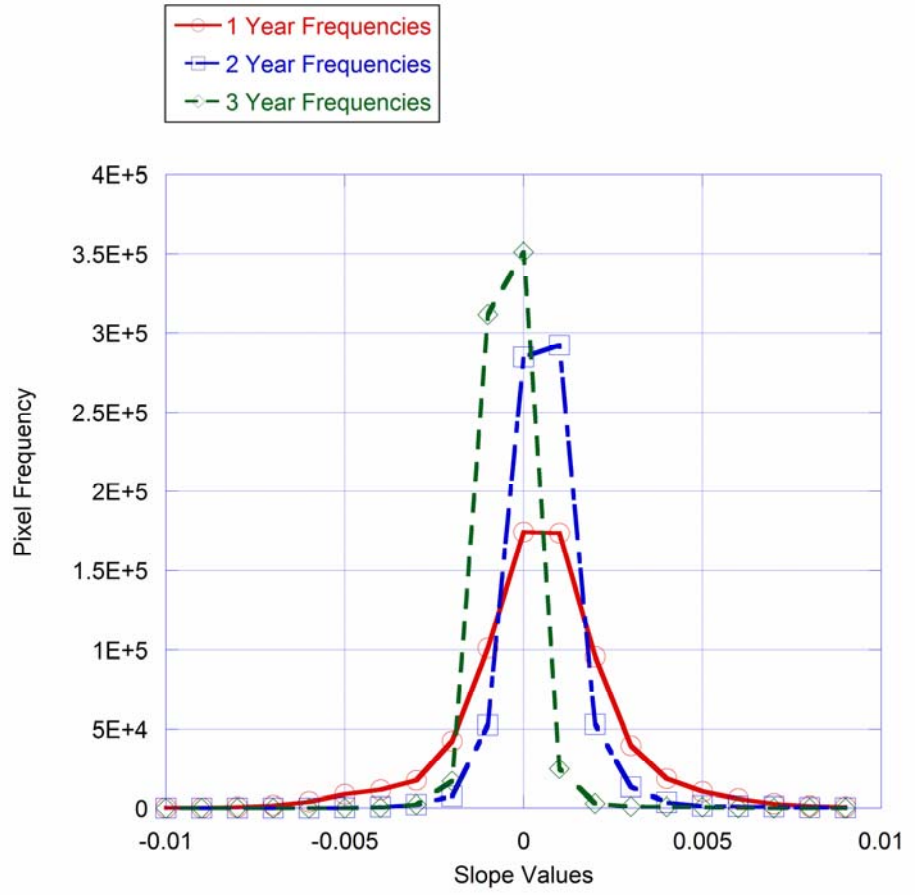

Fig. 4.6 Distribution of values for different recovery periods for South Florida region

Fig. 4.6 clearly shows how the kurtosis increased from the one-year recovery period to the three-year, whereas the mean of the curve approached zero. At the mean time, the skewness of the one-year curve toward positive value shifted toward the left with increasing length of the recovery period. These results show that the recovery rate was more widespread for the whole study area during the first year after the hurricanes, and most regions recovered back to pre-hurricane levels within two years. Further, after three years of recovery, almost all the study area had returned to normal levels with most *b* values approaching zero. Only a small portion of regions were still

recovering after three years. Expressing the recovery rate as $\Delta NDVI \cdot yr^{-1}$ could make the recovery rate more meaningful; in this way, the slope values range for Fig. 4.3, 4.4, 4.5 would range from -0.138 to -0.138 $\Delta NDVI \cdot yr^{-1}$.

The mean recovery rates for mangroves using the mask data in Fig 3.2 were subtracted separately from those slope images (Fig 4.3, 4.4, 4.5) for each time series, and the result are shown in Fig. 4.7. The initial value shows the mean recovery rate of the pre-hurricane period, and the middle values shows the average recovery rates for mangroves within different lengths of time periods and the last values show the mean recovery rates for the remaining post-recovery periods.

In Fig. 4.7, the mangrove recovery rate for the pre-hurricane period was 0.00248 $\Delta NDVI \cdot yr^{-1}$, which demonstrates that during the pre-hurricane period, there was very little change. The first year after Hurricane Wilma showed the highest recovery rate (0.0782 $\Delta NDVI \cdot yr^{-1}$), which indicates a high recovery period in mangroves for the first year after Hurricane Wilma. The recovery rate dropped to 0.0370 $\Delta NDVI \cdot yr^{-1}$ for the time period of two years after Hurricane Wilma, which shows a more moderate level of recovery. After three years, the recovery rate (0.018 $\Delta NDVI \cdot yr^{-1}$) was nearly zero, illustrating that the recovery was not intensive in this time period. This result reveals that for mangroves, the most intensive recovery period occurred during the first year after Hurricane Wilma, and the recovery rate decreased for longer recovery time series. The total recovery period appears to have lasted two to three years.

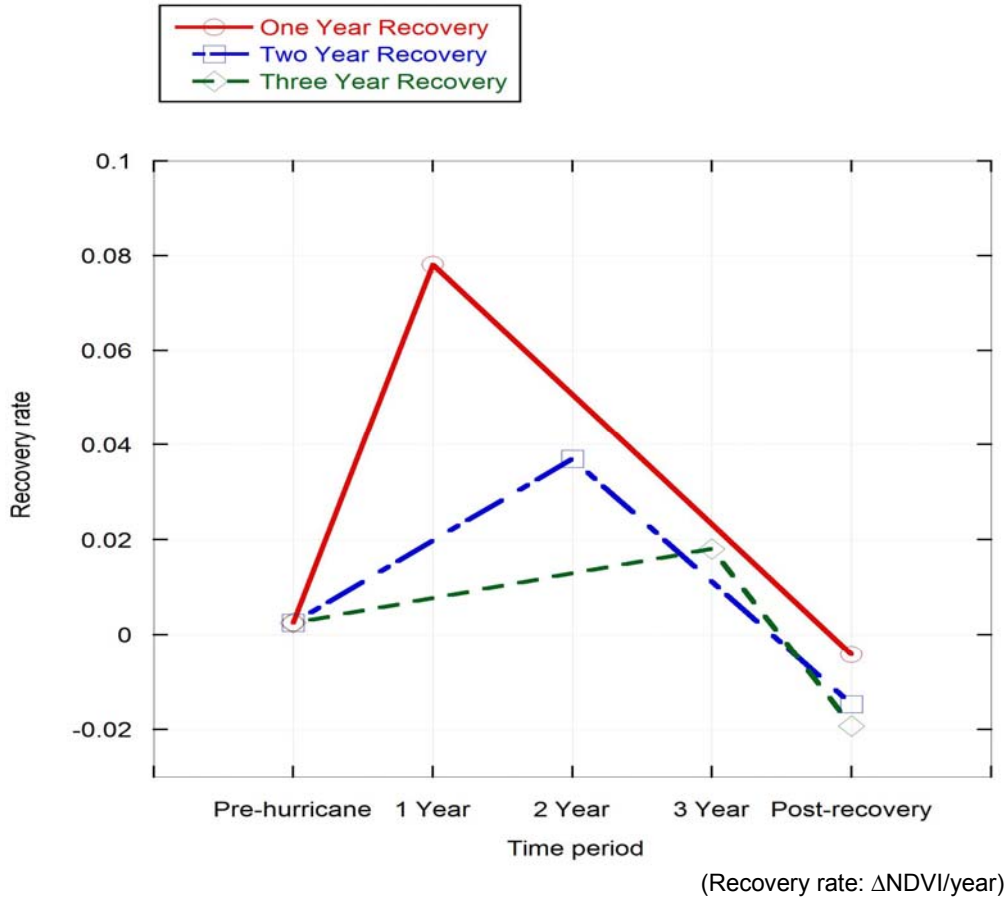

Fig. 4.7 Plot of recovery rate extracted from mangrove mask (shown in Fig. 3.2) for three recovery periods

4.3 Unsupervised Classification

The unsupervised classification for the layer stack of three slope images is shown in Fig. 4.8. In this figure, the higher-class values indicate higher recovery intensity while the lower-class values indicate lower recovery intensity. From the spatial distribution shown in Fig. 4.8, the higher-class values appeared mostly along the coastline in the southern part of the study area where most of mangroves are, as well as the southern part of Lake Okeechobee where is the Everglades Agriculture Area – in which the dominant crop type is sugarcane. The highest-class value indicates a high recovery rate as well as a long recovery period. Along with mangroves, sugarcane is

also one of the most vulnerable vegetation types; it is especially susceptible to strong wind force, such as hurricanes, which causes the termination of stalk growth, metabolic depletion, and reduced assimilation (Moore et al. 1985). The lower values were clustered in Lake Okeechobee; since there is little vegetation in this water body, the influence of hurricanes was quite minor. The relationship between recovery rates with land-cover types is analyzed below.

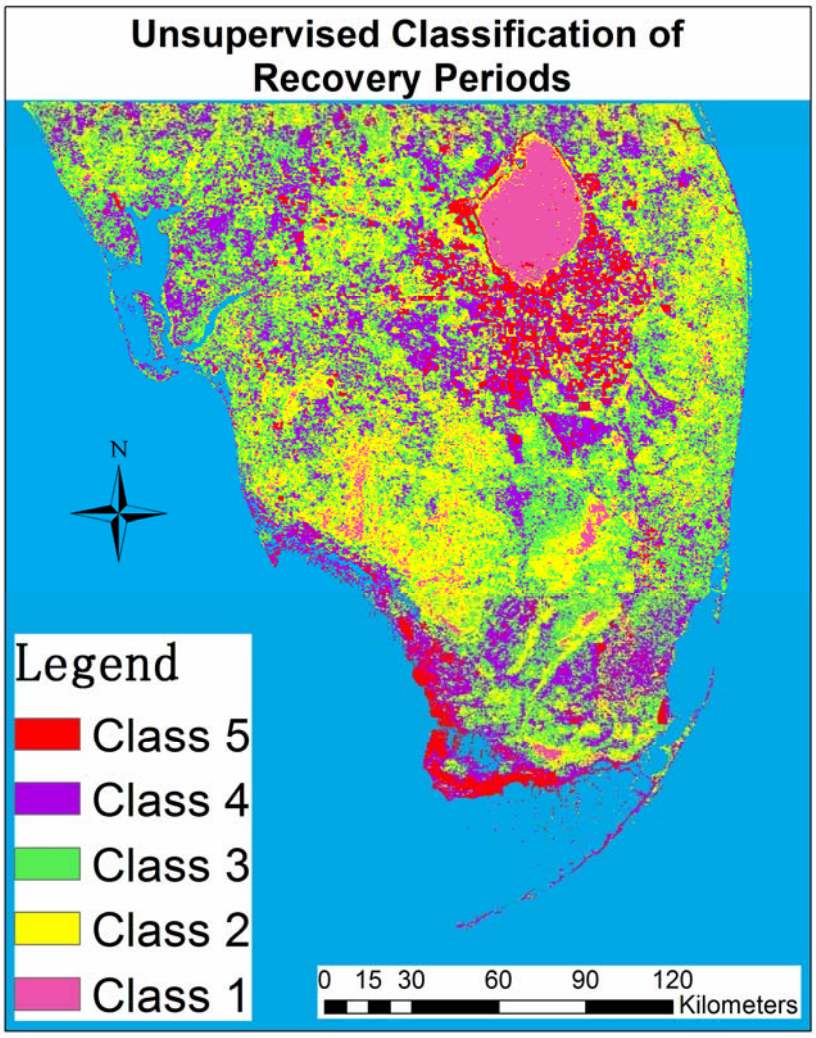

Fig. 4.8 Unsupervised classification result for the layer stack of three recovery periods with five classes (class 5 indicates the highest recovery rate and class 1 indicates the lowest)

4.4 Comparison

The spatial association between different land-cover types and recovery rates is presented in the matrix (Table 4.2), which shows the percentages of each land-cover type in different classes. In this chart, the 100.00% from Broadleaved Evergreen Forest – Closed Canopy appeared in Class 5, whereas 53.00% from Broadleaved Deciduous Forest appeared in Class 4 and 20.00% in Class 5. Both Broadleaved Forests had higher percentages in Class 4 and 5, which showed the high recovery rate for these two kinds of land cover, but the Broadleaved Evergreen Forest seems to have a higher recovery rate than the Broadleaved Deciduous Forest. Both Needleleaved Evergreen Forest – Closed Canopy and Needleleaved Evergreen Forest – Open Canopy showed the highest percentage of falling in Class 3 (44.01% of closed canopy and 48.48% of open canopy) and showed a moderate recovery rate. The highest percentage of Mixed Broadleaved or Needleleaved Forest lies in Class 4 (38.64%), which is in between the Broadleaved and Needleleaved. Broadleaved Evergreen Shrubland and Mixed Broadleaved and Needleleaved Dwarf-Shrubland displayed some difference between each other, the former having the highest percentage in Class 3 (43.03%) and the latter having the highest percentage in Class 4 (58.02%). Grassland and Grassland with a Sparse Tree Layer both have a similar highest percentage in Class 3. For Croplands, higher percentages were found in Class 3 (35.92%) and Class 4 (30.88%). For Unconsolidated Material Sparse Vegetation, the majority of pixels were found in Class 3 (41.33%) and Class 4 (36.18%). Urban and Built-up type showed highest percentage in Class 3 (52.44%), while Consolidated Rock Sparse Vegetation mostly appeared in Class 2 (34.24%) and 3 (28.39%). Water-body type had its highest percentage in Class 1 (46.75%), which shows a low recovery rate for this land-cover type as expected. Herbaceous Wetlands had the

highest percentage in Class 3 (40.26%) and second highest in Class 2 (34.70%). Mangroves showed its higher percentages in Class 4 (32.67%) and Class 5 (30.89%). From the results, some patterns could be found among different land-cover types. The Broadleaved forest had a higher recovery rate than the Needleleaved forest, and the forest land-cover types in total had higher rates than the shrubland and grassland land-cover types. Similarities could be found in the association between land-cover types and recovery rates with similar land-cover types (i.e., between Broadleaved Evergreen Forest and Broadleaved Deciduous Forest and Needleleaved Evergreen Forest with either open or closed canopy as well as Grassland), which supports this method. In the current thesis, some different land-cover types may share a similar recovery rate with others (i.e., between Needleleaved Evergreen Forest and Broadleaved Evergreen Shrubland, etc.), demonstrating that the recovery rate may not be a good parameter by which to classify land-cover types.

	Class 1	Class 2	Class 3	Class 4	Class 5
Broadleaved Evergreen Forest – Closed Canopy	0.00%	0.00%	0.00%	0.00%	100.00%
Broadleaved Deciduous – Closed Canopy	7.00%	7.00%	13.00%	53.00%	20.00%
Needleleaved Evergreen Forest – Closed Canopy	1.83%	26.87%	44.01%	25.74%	1.56%
Needleleaved Evergreen Forest – Open Canopy	0.63%	22.76%	48.48%	26.97%	1.16%
Mixed Broadleaved or Needleleaved Forest	2.37%	17.97%	25.08%	38.64%	15.93%
Broadleaved Evergreen Shrubland	2.48%	24.13%	43.03%	29.20%	1.17%
Mixed Broadleaved and Needleleaved Dwarf-Shrubland	0.00%	8.64%	33.33%	58.02%	0.00%
Grassland	2.78%	26.64%	42.43%	26.29%	1.86%
Grassland with a Sparse Tree Layer	0.66%	23.89%	49.01%	25.78%	0.66%
Cropland	2.21%	21.74%	35.92%	30.88%	9.25%
Unconsolidated Material Sparse Vegetation	1.13%	18.72%	41.33%	36.18%	2.63%
Urban and Built-up	1.62%	24.81%	52.44%	19.52%	1.62%
Consolidated Rock Sparse Vegetation	9.26%	34.24%	28.39%	14.56%	13.55%
Water bodies	46.75%	21.56%	17.89%	8.73%	5.07%
Herbaceous Wetlands	3.95%	34.70%	40.26%	18.46%	2.62%
Mangroves	1.62%	14.15%	20.67%	32.67%	30.89%

Table 4.2 Percentages of each land cover type matching with different classes (red labels mark the highest percentage of this kind of land cover, and the yellow labels show the second highest)

Chapter 5

Discussion and Conclusions

Large physical disturbances like hurricanes will cause different levels of damage in different vegetation types. In 2005, two hurricanes – Hurricane Katrina and Hurricane Wilma hit the South Florida region consecutively and induced significant damage on both built structures and the natural environment (especially vegetation). Since the two hurricanes occurred within a markedly short period, their effects might not be easily separated. A possible solution might be using the time period in between the two hurricanes to compare changes after each. In the South Florida region, Hurricane Katrina first made landfall as a hurricane and then degraded into a tropical storm (slower than 120 $km \cdot hr^{-1}$) while crossing Florida. In contrast, Hurricane Wilma was reached category 3 ($178km \cdot hr^{-1}$ – $209km \cdot hr^{-1}$), which was stronger and caused more damage than Hurricane Katrina in the study region (www.nhc.noaa.gov).

Wind damage, storm surges, and sediment deposition are the three main ways that hurricanes affect vegetation (Smith et al. 2009). The first two factors might cause several immediate effects – fallen trees, broken stems, sediment deposition and soil compaction – and can result in tree mortality and the inability of seedling to grow, which will have a long-term influence on vegetation recovery rates. Both immediate and long-term damage on vegetation would lower the photosynthetic activity, which makes the NDVI an effective parameter for evaluating damaged vegetation visible to satellite sensors. Despite the many studies that have examined the immediate impact of hurricanes on vegetation or recovery rates after fires, relatively few have analyzed either long-term effects or the recovery patterns of vegetation. This present thesis attempts to fill this research gap by using 8-day interval NDVI time series (2001 to

2010) derived from MODIS to study the recovery rates (through OLS slope analysis) of vegetation in South Florida following Hurricane Wilma.

The resulting images that represent the recovery rates for different time periods indicate that the values for the pre-hurricane period were near zero (Fig. 4.3, Page 31). It also shows higher frequencies of positive values ($b>0$) for recovery periods (Fig. 4.3, 4.4, 4.5, Page 31, 32, 33). The distribution of values (Fig. 4.6, Page 34) for the three different lengths of recovery periods shows the decrease of frequencies of positive values as the recovery period extends. The conclusion could be made that for the first year after Hurricane Wilma, this region experienced the most intensive recovery rate; this time period also featured the most spread-out recovery region of all time periods. After two years' recovery, most of the region returned to its pre-hurricane level; in terms of phenology, the region returned to its pre-hurricane level three years later.

Data on mangroves was extracted for different recovery lengths and is displayed separately. Fig. 4.7 (Page 36) shows a recovery pattern with an intensive recovery rate during the first year after the hurricanes. This result not only demonstrates the high recovery rate and indicates severe damage to the mangroves after Hurricane Wilma, it agrees with the vulnerability mentioned in previous studies (Omo-Irabor et al. 2011; Rodgers, Murrah, and Cooke 2009; Giri et al. 2007). The recovery rate of the period two years after hurricanes was still higher than the pre-hurricane level, and after three years, the mangroves were almost back to normal in terms of phenological behavior. This result indicates that the recovery pattern for mangroves after hurricanes might be different than after fires, since van Leeuwen (2008) concluded that, in terms of phenological behavior, the recovery of mangroves needs less than five years.

Compared with previous vegetation recovery studies, the OLS method presented in the current thesis provided a robust way to detect the recovery rates and patterns. First, this method is simple and easily understood, and by extracting recovery slope values for each pixel, information is more detailed than a grouped region with different pixels, which was used by van Leeuen (2008). Second, by using this method, the seasonal variance could be eliminated, which could also decrease the effect from inter-annual variance that may appear when using phenological metrics to study recovery rates (van Leeuwen 2008). Overall, using NDVI time series to detect vegetation recovery patterns through OLS slope analysis appears to provide a reliable tool for vegetation recovery studies. One of the limitations of this method appeared when using the linear function to simulate the recovery pattern of vegetation. That is because the natural pattern for vegetation recovery might shift from an initial high intensive to a subsequently lower intensity. In this sense, other functions, especially the exponential function, might better fit recovery rate trend. Future work could be performed using other functions to imitate the recovery patterns.

The NDVI time series derived from MODIS Terra satellite contain noise, most likely from sub-pixel clouds, incomplete or inconsistent atmospheric correction bi-directional effects and calibration issues. Although the MODIS 8-day images are MVC product, noise caused by other factors could remain in the time series. To obtain higher quality data, the inverse Fourier Fitting method was used to de-noise the NDVI time series in order to obtain a smoothed time series. Previous studies agreed that 50% to 90% variability could be captured in the first two harmonics, and three to five harmonics could maintain the phenological cycle for a one-year length time series. In the present thesis, the results of the correlation analysis showed that the best coefficient of determination (r^2) between NDVI data and smoothed series was found

when 16 harmonics was used. This indicates that an inverse-FFT that utilizes 16 harmonics is most suitable for extracting signals from noise in a ten-year NDVI time series. Qualitative evidence (Table 4.1, Page 29) also suggests that smoothing approach preserved both annual and seasonal trends. Based on the manual technique support from the Idrisi manual as well as the theoretical support from Bloomfield (2005) , the suitable harmonics numbers for inverse Fourier fitting method to smooth a NDVI time series should depend on the length of the time series and should amount to no more than twice the number of years. The results shown in the present thesis are consistent with this principle. For further studies using the inverse Fourier fitting smoothing method, the length of the time series should be taken into consideration. Linear regression could provide an effective way to show the different levels of fitting through an examination of the correlation coefficient between the filtered data and the original time series. In this way, the most suitable harmonics number to smooth the time series could be decided by choosing the best fit.

Different vegetation types have unique reactions to environmental disturbances, and recovery mechanisms that help them return to their pre-disturbance level within a certain time period. Trees might have more severe reactions to wind damage and storm surges, whereas grassland might be more influenced by long-term effects like sediment deposition. For recovery mechanisms, some species might rely on a seed banks (e.g., grassland in arid and semiarid ecosystems [Scott et al. 2012]) while other species might simply recover through sprouting, even from an uprooted tree (e.g., Eastern hemlock [McKee et al. 2007]). The difference between land-cover types could result in different recovery rates, a conclusion supported by the present thesis.

The relationship between land-cover types and recovery rate was examined by using a five-class slope values image (Fig. 4.8, Page 37) with the land-cover map (Fig. 2.5, Page 17). Table 4.2 (Page 40) indicates the percentage of each land-cover type that appears in each class. The results illustrate the relationship between land-cover types and recovery rates and show that similar land-cover types had similar recovery rates. For example, broadleaved forests had higher recovery rates (Class 4, 5), and the needleleaved forest had a similar moderate recovery rate (Class 2, 3, 4) regardless of open or closed canopies. Similar rates were also found in grassland and grassland with sparse trees.

These results demonstrate the efficacy of using the OLS slope method to detect the recovery patterns through NDVI time series. But since different land-cover types might have similar recovery rates, (e.g., needleleaved forest and broadleaved evergreen shrubland), the results in the present thesis show that the OLS method might not be the most effective way to separate different land-cover types. Further analysis using a different classification approach may be warranted. Another interesting phenomenon appeared in the relationship between mean and standard deviation of NDVI time series extracted from the mangroves data (Fig 4.1, Page 26). Low values frequently appeared with the peak of NDVI, which indicates that the data points tend to be very close to the mean. High standard deviation appeared near the bottom values, indicating that the data points are spread out over a large range of values. The peak of NDVI indicates the end of the wet season, during which water availability is generally spatially homogeneous; this helps to explain the low variance. But during the end of the dry season (the minimum NDVI) when vegetation starts to become green, the availability of water varies in different regions; this appears to explain the high variance. Future studies could be performed to examine other

possible factors (location, species types or cloud cover) that might influence the recovery rate for mangroves or other land-cover types. This method could also be used with different kinds of disturbances, such as droughts and anthropogenic disturbances (e.g., deforestation or desertification).

Several studies have indicated that the biomass of the canopies was most likely still recovering, even though they had already recovered phenologically. Sarmiento et al. (2010) studied mangrove biomass recovery in the Everglades after Hurricane Wilma by detecting carbon dioxide (CO_2). They found that after about four years' recovery the flux of carbon dioxide over the entire year of 2009 had not yet reached pre-disturbance values yet (Sarmiento et al. 2010). This result shows that annual productivity, which is related to energy and materials exchange, might not be closely related to the phenological cycle during post-disturbance recovery. This also suggests that this method might be not suitable for productivity studies.

Other studies have discussed the advantages of using EVI instead of NDVI, because the former reduces the adverse effects of atmospheric variability and soil background. Moreover, the EVI has improved sensitivity to high biomass regions and improved vegetation monitoring capability through the de-coupling of the canopy background signal and a reduction in atmospheric influences (Matsushita et al. 2007). Although the EVI has its own advantages, the blue band image provided by MODIS only has a spatial resolution of 500 m, which significantly reduces the spatial detail of EVI time series. As spatial resolution was considered important in order to analyze different patterns, MODIS NDVI was chosen in the present thesis.

References

Bloomfield, P. 2005. *Fourier Analysis of Time Series: An Introduction, Second Edition.* Wiley.

Cakir, H. I., S. Khorram, and S. A. C. Nelson. 2006. Correspondence Analysis for Detecting Land Cover Change. *Remote Sensing of Environment* 102 (3-4):306-317.

Campbell, R. J., C. W. Campbell, J. Crane, C. Balerdi, and S. Goldweber. 1993. Hurricane-Andrew Damages Tropical Fruit Crops in South Florida. *Fruit Varieties Journal* 47 (4):218-225.

Castaneda-Moya, E., R. R. Twilley, V. H. Rivera-Monroy, K. Zhang, S. E. Davis, III, and M. Ross. 2011. Sediment and Nutrient Deposition Associated with Hurricane Wilma in Mangroves of the Florida Coastal Everglades. *Estuaries and Coasts* 33 (1):45-58.

Chen, J., P. Jonsson, M. Tamura, Z. H. Gu, B. Matsushita, and L. Eklundh. 2004. A Simple Method for Reconstructing a High-Quality NDVI Time-Series Data Set based on the Savitzky-Golay filter. *Remote Sensing of Environment* 91 (3-4):332-344.

Chu, H.-J., Y.-P. Lin, Y.-L. Huang, and Y.-C. Wang. 2009. Detecting the Land-Cover Changes Induced by Large-Physical Disturbances Using Landscape Metrics, Spatial Sampling, Simulation and Spatial Analysis. *Sensors* 9 (9):6670-6700.

Cihlar, J., R. Latifovic, J. Chen, J. Beaubien, and Z. Li. 2000. Selecting Representative High Resolution Sample Images for Land Cover Studies. Part 1: Methodology. *Remote Sensing of Environment* 71 (1):26-42.

Cushman, K., M. Ozores-Hampton, E. Simonne, and E. McAvoy. 2006. Yields of Hurricane-Damaged Tomato Crops in Southern Florida. In *Proceedings of the 119th Annual Meeting of the Florida State Horticultural Society*, 234-239. Winter Haven: Florida State Horticultural Soc.

Duever, M. J., J. E. Carlson, J. F. Meeder, L. C. Duever, L. H. Gunderson, L. A. Riopelle, T. R. Alexander, R. L. Myers, and D. P. Spangler. 1986. The Big Cypress National Preserve. *Research Report of the National Audubon Society*:i-xvii, 1-455.

Eastman J.R. 2009. *IDRSI Taiga: Guide to GIS and Image Processing.* Clark Labs.

Fuller, D. O. 1998. Trends in NDVI Time Series and Their Relation to Rangeland and Crop Production in Senegal, 1987-1993. *International Journal of Remote Sensing* 19 (10): 2013-2018.

Geerken, R., B. Zaitchik, and J. P. Evans. 2005. Classifying Rangeland Vegetation Type and Coverage from NDVI Time Series using Fourier Filtered Cycle Similarity. *International Journal of Remote Sensing* 26 (24):5535-5554.

Geerken, R. A. 2009. An Algorithm to Classify and Monitor Seasonal Variations in Vegetation Phenologies and Their Inter-annual Change. *Isprs Journal of Photogrammetry and Remote Sensing* 64 (4):422-431.

Giri, C., B. Pengra, Z. Zhu, A. Singh, and L. L. Tieszen. 2007. Monitoring Mangrove Forest Dynamics of the Sundarbans in Bangladesh and India Using Multi-temporal Satellite Data from 1973 to 2000. *Estuarine Coastal and Shelf Science* 73 (1-2):91-100.

Goetz, S. J., G. J. Fiske, and A. G. Bunn. 2006. Using Satellite Time-Series Data Sets to Analyze Fire Disturbance and Forest Recovery across Canada. *Remote Sensing of Environment* 101 (3):352-365.

Hasegawa, K., H. Matsuyama, H. Tsuzuki, and T. Sweda. 2009. Improving the Estimation of Leaf Area Index by Using Remotely Sensed NDVI with BRDF Signatures. *Remote Sensing of Environment* 114 (3):514-519.

Jakubauskas, M. E., D. R. Legates, and J. H. Kastens. 2001. Harmonic Analysis of Time-Series AVHRR NDVI Data. *Photogrammetric Engineering and Remote Sensing* 67 (4):461-470.

Jeganathan, C., J. Dash, and P. M. Atkinson. 2010. Mapping the Phenology of Natural Vegetation in India Using a Remote Sensing-Derived Chlorophyll Index. *International Journal of Remote Sensing* 31 (22):5777-5796.

Kamthonkiat, D., C. Rodfai, A. Saiwanrungkul, S. Koshimura, and M. Matsuoka. 2011. Geoinformatics in Mangrove Monitoring: Damage and Recovery after the 2004 Indian Ocean Tsunami in Phang Nga, Thailand. *Natural Hazards and Earth System Sciences* 11 (7):1851-1862.

Kefi, M., K. Yoshino, and Y. Setiawan. 2012. Assessment and Mapping of Soil Erosion Risk by Water in Tunisia Using Time Series MODIS Data. *Paddy and Water Environment* 10 (1):59-73.

Krauss, K. W., T. W. Doyle, R. R. Twilley, T. J. Smith, K. R. T. Whelan, and J. K. Sullivan. 2005. Woody Debris in the Mangrove Forests of South Florida. *Biotropica* 37 (1):9-15.

Los, S. O., G. J. Collatz, P. J. Sellers, C. M. Malmstrom, N. H. Pollack, R. S. DeFries, L. Bounoua, M. T. Parris, C. J. Tucker, and D. A. Dazlich. 2000. A Global 9-yr Biophysical Land Surface Dataset from NOAA AVHRR Data. *Journal of Hydrometeorology* 1 (2):183-199.

Ma, M. G., and F. Veroustraete. 2006. Reconstructing Pathfinder AVHRR Land NDVI Time-Series Data for the Northwest of China. In *Natural Hazards and Oceanographic Processes from Satellite Data*, 835-840.

Matsushita, B., W. Yang, J. Chen, Y. Onda, and G. Qiu. 2007. Sensitivity of the Enhanced Vegetation Index (EVI) and Normalized Difference Vegetation Index (NDVI) to Topographic Effects: A Case Study in High-Density Cypress Forest. *Sensors* 7 (11):2636-2651.

McKee, K. L., J. E. Rooth, and I. C. Feller. 2007. Mangrove Recruitment after Forest Disturbance is Facilitated by Herbaceous Species in the Caribbean. *Ecological Applications* 17 (6):1678-1693.

Omo-Irabor, O. O., S. B. Olobaniyi, J. Akunna, V. Venus, J. M. Maina, and C. Paradzayi. 2011. Mangrove Vulnerability Modelling in Parts of Western Niger Delta, Nigeria Using Satellite Images, GIS Techniques and Spatial Multi-Criteria Analysis (SMCA). *Environmental Monitoring and Assessment* 178 (1-4):39-51.

Parmentier, I., R. J. Harrigan, W. Buermann, E. T. A. Mitchard, S. Saatchi, Y. Malhi, F. Bongers, W. D. Hawthorne, M. E. Leal, S. L. Lewis, L. Nusbaumer, D. Sheil, M. S. M. Sosef, K. Affum-Baffoe, A. Bakayoko, G. B. Chuyong, C. Chatelain, J. A. Comiskey, G. Dauby, J. L. Doucet, S. Fauset, L. Gautier, J. F. Gillet, D. Kenfack, F. N. Kouame, E. K. Kouassi, L. A. Kouka, M. P. E. Parren, K. S. H. Peh, J. M. Reitsma, B. Senterre, B. Sonke, T. C. H. Sunderland, M. D. Swaine, M. G. P. Tchouto, D. Thomas, J. Van Valkenburg, and O. J. Hardy. 2011. Predicting Alpha Diversity of African Rain Forests: Models Based on Climate and Satellite-Derived Data do not Perform better than a Purely Spatial Model. *Journal of Biogeography* 38 (6):1164-1176.

Patil, P., S. Singh, and V. K. Dadhwal. 2012. Above Ground Forest Phytomass Assessment in Southern Gujarat. *Journal of the Indian Society of Remote Sensing* 40 (1):37-46.

Petit, C., T. Scudder, and E. Lambin. 2001. Quantifying Processes of Land-Cover Change by Remote Sensing: Resettlement and Rapid Land-Cover Changes in South-Eastern Zambia. *International Journal of Remote Sensing* 22 (17):3435-3456.

Piou, C., I. C. Feller, U. Berger, and F. Chi. 2006. Zonation Patterns of Belizean Offshore Mangrove Forests 41 Years after a Catastrophic Hurricane. *Biotropica* 38 (3):365-374.

Rocchini, D., and A. Vannini. 2010. What is up? Testing Spectral Heterogeneity versus NDVI Relationship using Quantile Regression. *International Journal of Remote Sensing* 31 (10):2745-2756.

Rodgers, J. C., III, A. W. Murrah, and W. H. Cooke. 2009. The Impact of Hurricane Katrina on the Coastal Vegetation of the Weeks Bay Reserve, Alabama from NDVI Data. *Estuaries and Coasts* 32 (3):496-507.

Sarmiento, D., J. Barr, V. Engel, J. Fuentes, T. J. Smith, and J. Zieman. 2010. Mangrove Forest Recovery in the Everglades following Hurricane Wilma. *LTER Network News* Vol. 22 No.2 (Network News Fall 2009).

Scott, A. J., and J. W. Morgan. 2012. Resilience, Persistence and Relationship to Standing Vegetation in Soil Seed Banks of Semi-Arid Australian Old Fields. *Applied Vegetation Science* 15 (1):48-61.

Sellers, P. J., S. O. Los, C. J. Tucker, C. O. Justice, D. A. Dazlich, G. J. Collatz, and D. A. Randall. 1994. A Revised Land Surface Parameterization (SiB2) for Atmospheric GCMs. Part II: The Generation of Global Fields of Terrestrial Biophysical Parameters from Satellite Data. *Journal of Climate* 9:706-737.

Smith, T. J., III, G. H. Anderson, K. Balentine, G. Tiling, G. A. Ward, and K. R. T. Whelan. 2009. Cumulative Impacts of Hurricanes on Florida Mangrove Ecosystems: Sediment Deposition, Storm Surges and Vegetation. *Wetlands* 29 (1):24-34.

Tucker, C. J. 1979. Red and Photographic Infrared Linear Combinations for Monitoring Vegetation. *Remote Sensing of Environment* 8 (2):127-150.

Tucker, C. J., D. A. Slayback, J. E. Pinzon, S. O. Los, R. B. Myneni, and M. G. Taylor. 2001. Higher Northern Latitude Normalized Difference Vegetation Index and Growing Season Trends from 1982 to 1999. *International Journal of Biometeorology* 45 (4):184-190.

Turner, M. G. 1987. Spatial Simulation of Landscape Changes in Georgia: A comparison of 3 transition models. *Landscape Ecology* 1 (1):29-36.

van Leeuwen, W. J. D. 2008. Monitoring the Effects of Forest Restoration Treatments on Post-Fire Vegetation Recovery with MODIS Multitemporal Data. *Sensors* 8 (3):2017-2042.

Verhoef, W., M. Menenti, and S. Azzali. 1996. A Colour Composite of NOAA-AVHRR-NDVI Based on Time Series Analysis (1981-1992). *International Journal of Remote Sensing* 17 (2):231-235.

Vrieling, A., K. M. de Beurs, and M. E. Brown. 2011. Variability of African farming systems from phenological analysis of NDVI time series. *Climatic Change* 109 (3-4):455-477.

Wells, S. 2006. In the Front Line: Shoreline Protection and Other Ecosystem Services from Mangroves and Coral Reefs. *WCMC Biodiversity Series* 24:1-33.

Wittenberg, L., D. Malkinson, O. Beeri, A. Halutzy, and N. Tesler. 2007. Spatial and Temporal Patterns of Vegetation Recovery following Sequences of Forest Fires in a Mediterranean Landscape, Mt. Carmel Israel. *Catena* 71 (1):76-83.